AMPAR/TARP stoichiometry differentially modulates channel properties

Federico Miguez-Cabello[1], Nuria Sánchez-Fernández[1], Natalia Yefimenko[1], Xavier Gasull[1,2], Esther Gratacòs-Batlle[1] and David Soto[1,2,*]

[1] Laboratori de Neurofisiologia, Departament de Biomedicina, Facultat de Medicina i Ciències de la Salut, Institut de Neurociències, Universitat de Barcelona, Barcelona, Spain.

[2] Institut d'Investigacions Biomèdiques August Pi i Sunyer (IDIBAPS), Barcelona, Spain.

* Corresponding author:
Dr. David Soto
Laboratori de Neurofisiologia. Departament de Biomedicina
Facultat de Medicina - Universitat de Barcelona
Casanova 143, 08036
Barcelona
Spain
e-mail: davidsoto@ub.edu

Keywords: AMPAR, TARP, stoichiometry, cerebellar granule cells, channel conductance, desensitization, out-side out, polyamine block.

NUMBER OF WORDS: 7817

Summary: 150

Introduction: 748

Results: 2964

Discussion: 2079

Methods: 614

Figure legends: 1265

NUMBER OF PAGES: 49

NUMBER OF FIGURES: 7

NUMBER OF REFERENCES: 64

Acknowledgements: We would like to thank Francesc Sureda (Universitat Rovira i Virgili) for technical assistance with cerebellar granule cell cultures and Jon Giblin for English revision.

Declaration of interests: The authors declare no competing interests.

Author ORCID numbers:

Esther Gratacòs-Batlle: 0000-0001-8093-3713

Xavier Gasull: 0000-0002-6154-8323

David Soto: 0000-0001-7995-3805

Summary

AMPARs control fast synaptic communication between neurons and their function relies on auxiliary subunits, which importantly modulate channel properties. Although it has been suggested that AMPARs can bind to TARPs with variable stoichiometry, little is known about the effect that this stoichiometry exerts on certain AMPAR properties. Here we have found that AMPARs show a clear stoichiometry dependent modulation although AMPARs still need to be fully saturated with TARPs to show some typical TARP-induced characteristics (i.e. an increase in channel conductance). We also have uncovered important differences in the stoichiometric modulation between calcium-permeable and calcium-impermeable AMPARs. Moreover, in heteromeric AMPARs, TARP positioning in the complex is important to exert certain TARP-dependent features. Finally, by comparing data from recombinant receptors with endogenous AMPAR currents from cerebellar granule cells, we have determined a likely functional stoichiometry of 2 TARPs associated with GluA2 subunits in the somatic AMPARs found in this cell type.

Introduction

Glutamate is a crucial neurotransmitter in the central nervous system (CNS) since it mediates the vast majority of the fast-excitatory synaptic transmission acting on postsynaptic ionotropic glutamate receptors. Among these, α-amino-3-hydroxy-5-methyl-4-isoxazolepropionic acid (AMPA) receptors (AMPARs) are fundamental players in the synaptic course besides their pivotal role as regulators of synaptic plasticity. AMPARs are homo or heterotetrameric structures composed of four GluA subunits (GluA1-4) (Traynelis et al. 2010) and their biophysical properties are dramatically changed depending on the subunits that conform the ion channel, with the presence or absence of the GluA2 subunit a critical determinant of channel properties. In particular, while GluA2-lacking AMPARs are permeable to both Na^+ and Ca^{2+} ions, AMPARs containing the GluA2 subunit are impermeable to Ca^{2+}. GluA2-containing AMPARs do not allow Ca^{2+} influx through the channel due to an RNA editing process that results in the replacement of an Arginine with a Glutamine residue in the cation selectivity filter region of this subunit at the so-called Q/R site (Hollmann et al. 1991; Burnashev et al. 1992). This RNA editing process is exclusive for this GluA subunit and occurs in 99% of native GluA2 subunits (Geiger et al. 1995; Kawahara et al. 2003). This change not only affects Ca^{2+} permeability but also single-channel conductance, which is decreased in GluA2-containing AMPARs mainly due to the lack of Ca^{2+} permeability (Swanson et al. 1995). This editing at the Q/R site also impairs the blocking effect of endogenous polyamines on these receptors at depolarized membrane potentials compared to GluA2-lacking AMPARs, which are strongly blocked by spermine (Bowie and Mayer, 1995; Kamboj et al. 1995; Koh et al. 1995). Thus, AMPARs are frequently classified as Ca^{2+}-impermeable *vs.* Ca^{2+}-permeable (CI *vs.* CP-AMPARs – or GluA2-containing *vs.* GluA2-lacking. Finally, the Q/R editing of the GluA2 subunit powerfully influences AMPAR tetramerization and strongly disfavours formation of GluA2 homotetramers (Greger et al. 2003).

Although AMPAR gating – and also trafficking – properties are determined by their subunit composition, these features are also strongly dependent on AMPAR-

associated transmembrane proteins that behave as auxiliary subunits of the receptor. In the last 15 years, the number of interacting proteins that can act as modulatory partners of AMPARs has vastly increased. Stargazin and other TARPs (*Transmembrane AMPAR Regulatory Proteins*) were the first discovered proteins modulating AMPARs (Chen et al. 2000; Tomita et al. 2005). TARPs are one of the most studied AMPAR auxiliary proteins because of their indispensable role in neuronal physiology (*see (Payne 2008) for review*) and in different types of synaptic plasticity (Rouach et al. 2005; Louros et al. 2014; Sullivan et al. 2017; Louros et al. 2018). It is well-known that members of the TARP family can modify biophysical properties of AMPARs by increasing conductance, slowing down kinetics or diminishing polyamine block in CP-AMPARs (Priel et al. 2005; Soto et al. 2007). Furthermore, TARPs can modify AMPAR pharmacology such as kainate-evoked responses (Kott et al. 2007; Turetsky et al. 2005). However, much less is known about the number of TARP molecules that can be present in an AMPAR complex although AMPAR/TARP stoichiometry has been investigated by single-molecule subunit counting (Hastie et al. 2013) and electrophysiological studies that have demonstrated that AMPAR efficiency to kainate vary depending on the number of TARPs present in the receptor (Shi et al. 2009). More recently, functional studies together with high definition structural data have provided evidence for a favoured 2-TARP per AMPAR stoichiometry (Dawe et al. 2019; Herguedas et al. 2019). However, with only a small number of studies investigating AMPAR/TARP stoichiometry it is still not established whether TARPs can modulate AMPARs in a stoichiometry dependent manner.

In the present work we have determined how the number of TARP molecules per AMPAR complex modify the biophysical properties of these receptors in a stoichiometry dependent manner in both CP and CI-AMPARs. To approach this issue, we have used AMPAR/TARP fusion proteins to fix stoichiometries of 2 and 4 TARPs per AMPAR. Our results show a complex stoichiometry-dependent modulation with important differences observed between CP and CI-AMPARs. Moreover, we have attempted to reveal the endogenous functional AMPAR/TARP

126 stoichiometry in cerebellar granule cells (CGCs) by correlating results obtained in
127 recombinant AMPARs with recordings on CGC cultures. We have taken advantage
128 that this cerebellar neuronal type expresses a limited variety of GluA and TARP
129 subunits together with a lack of cornichons expression on the plasma membrane
130 (another important AMPAR auxiliary protein) (Schwenk et al. 2009; Shi et al. 2010).
131 We propose that 2 TARPs attached to GluA2 subunits determine functional
132 somatic AMPAR properties in CGCs.
133
134 **Results**
135 TARPs induce a gradual change in CP-AMPAR kinetics
136 AMPAR biophysical behaviour is strongly modulated by TARPs, which differentially
137 control AMPAR gating (Straub and Tomita, 2012; Haering et al. 2014; Jackson and
138 Nicoll, 2011; Greger et al. 2017). The prototypical TARP γ2 slows deactivation and
139 desensitization of AMPAR-mediated responses (Priel et al. 2005), as observed
140 with the other members of the TARP family (Soto et al. 2009). However, the
141 potential impact of different TARP stoichiometry on AMPAR function is vastly
142 unknown. We wondered about the degree of the slowdown of CP-AMPAR
143 responses in two different TARP stoichiometries to determine whether an
144 increasing number of TARP subunits present into the AMPAR complex modulates
145 channel properties in a gradual way or whether the presence of two TARP
146 molecules is enough to provide AMPARs with a TARPed behaviour. We studied
147 two fixed stoichiometries using the fusion protein GluA1:γ2, which comprises
148 GluA1 and γ2 in the same protein product. The functional validation of this
149 construct has been previously reported (Soto et al. 2014). We co-transfected
150 tsA201 cells with GluA1 and/or GluA1:γ2 in such a way that GluA1 homomeric CP-
151 AMPARs had zero, two or four TARPs per receptor. Then we extracted outside-out
152 patches from transfected cells and we applied a 10 mM glutamate step during 100
153 ms with a piezoelectric controller to acquire fast AMPAR-mediated currents.
154
155 We analysed desensitization kinetics of GluA1homomeric receptors in the absence
156 or the presence of 2 or 4 γ2 molecules. Desensitization of GluA1 in the presence of

the saturating concentration of glutamate – measured as the weighted time constant (τ_w) – showed a clear TARP dependence with an increase in desensitization time as the number of γ2 units in the complex increased (2.32 ± 0.16 ms, 3.77 ± 0.39 ms and 6.70 ± 0.41 ms for 0-TARPs, 2-TARPs and 4-TARPs respectively; $p<0.01$ for comparisons between all groups; student's *t*-test; Figure 1A-B).

In contrast to the well-defined step changes observed for desensitization kinetics, there was not a crystal-clear gradual change in steady state current (Figure 1C). A significant change was detected when the CP-AMPAR was fully saturated with TARPs (2.78 ± 1.04 % for 0-TARPs *vs.* 13.95 ± 1.85 % for 4-TARPs; $p<0.0001$; Mann Whitney *U*-test) although a gradual change cannot be discarded since a difference was observed between the 2-TARPs and 4-TARPs groups (5.58 ± 1.70 % for 2-TARPs *vs.* 13.95 ± 1.85 % for 4-TARPs; $p<0.01$; Mann Whitney *U*-test).

We next analysed the kinetics of the current activation (rise time) and observed that only fully TARPed GluA1 homomeric receptors presented a significant increase in the time to reach the peak current (0.46 ± 0.06 ms, 0.61 ± 0.12 ms and 0.67 ± 0.08 ms for 0-TARPs, 2-TARPs and 4-TARPs respectively; $p>0.05$ for all comparisons except $p=0.0167$ for 0-TARPs *vs.* 4-TARPs; Mann Whitney *U*-test; Figure 1D).

TARPs also speed the recovery from desensitization of AMPARs (Priel et al. 2005; Gill et al. 2012; Cais et al. 2014; Carbone and Plested, 2016) so we checked if this phenomenon was stoichiometry dependent. We applied paired pulses separated by 50 to 600 ms intervals to patches from cells expressing GluA1, GluA1+GluA1:γ2 or GluA1:γ2. Figure 2A shows typical recordings for the three conditions mentioned above. We then calculated the desensitization recovery rate and we observed a clear gradual effect, being the 2-TARPs condition half way between the slow recovery of 0-TARPs and the quicker recovery of 4-TARPs (Figure 2B). Specifically, we found time constants (τ) of 210.58 ± 1.2 ms for 0-TARPs, 194.57 ±

188 1.23 ms for 2-TARPs and 187.49 ± 1.65 ms for 4-TARPs (Figure 2C; n= 8, 15 and
189 9 respectively; p<0.01 for all comparisons; student's *t*-test).
190
191 CP-AMPAR polyamine block attenuation strongly depends on TARP dosage
192 An important canonical property of CP-AMPARs is the strong intracellular
193 polyamine block of the channel especially at depolarized potentials, which
194 translates into a characteristic inwardly rectifying current-voltage relationship
195 (Kamboj et al. 1995). This strong block by polyamines is attenuated as a
196 consequence of TARP modulation (Soto et al. 2007; Soto et al. 2009). Thus, we
197 investigated if this weakening of the block followed a stepwise pattern similar to the
198 one observed for desensitization kinetics. We observed a strong dependence on
199 the number of TARPs associated with the CP-AMPAR in such attenuation across
200 different membrane voltages (Figure 3A-B). The rectification index (RI; +60mV/-
201 60mV; Figure 3C) clearly demonstrates a stoichiometry dependence of TARP-
202 mediated attenuation of spermine block (0.056 ± 0.004 for 0-TARPs; 0.128 ± 0.011
203 for 2-TARPs and 0.274 ± 0.021 for 4-TARPs; p<0.0001 for comparisons between
204 all groups; student's *t*-test).
205
206 Given the results obtained in Figures 1-3, which supports the idea of a gradual
207 modulation of GluA1 homomeric receptors depending on the number of TARPs, we
208 wondered whether in the studied 2-TARPed condition a mixture of two distinct
209 populations of AMPARs – 0-TARPed and 4-TARPed – rather than a pure
210 population of heteromeric GluA1-GluA1:γ2 existed. This would account for the
211 intermediate phenotype observed in the recordings. Therefore, we decided to
212 transfect tsA201 cells with GluA1(Q) together with its edited variant GluA1(R) and
213 use the polyamine block as an indicator of the existence of an heteromeric
214 population. GluA1(Q) homomers are strongly blocked by polyamines and since
215 GluA1(R) homomers are strongly disfavoured, a linear response would be
216 indicative of a GluA1(Q)-GluA1(R) heteromeric receptor. We set the RI cut point as
217 0.7, considering a lower value in the responses as evidence for a considerable
218 contamination with GluA1(Q) homomers. We found that 80% of the responses

showed a RI >0.7 (8 out of 10 recordings). Importantly, when we co-transfected GluA1(Q):γ2 with GluA1(R) we observed RIs above 0.7 in all recorded patches (n=9), a percentage that did not differ from the TARPless condition (p=0.4737; Fisher's exact test). We examined the desensitization kinetics of these recordings to confirm the effect of γ2 in the complex. As detected with GluA1(Q) forms, in the GluA1(R)-containing receptors the weighted time constant (τ_w) of the TARPed receptor was slowed significantly compared with the TARPless receptor (2.87 ± 0.47 for 0-TARPs *vs.* 4.32 ± 0.46 for 2-TARPs; p<0.05; student's *t*-test) (data not shown) indicating that the results seen in the 2-TARPed conditions with GluA1(Q) were acquired most probably from a 2-TARPed population rather than two populations of TARPless and fully TARPed AMPARs.

<u>CP-AMPARs conductance increase by TARPs needs a fully saturated receptor</u>

We next performed non-stationary fluctuation analysis (NSFA) to obtain single-channel conductance and peak open probability from these macroscopic responses. Figure 4A shows representative responses from TARPless, 2 TARPed and 4 TARPed AMPARs together with their corresponding NSFA (Figure 4B). We obtained conductance values for TARPless GluA1 homomeric receptors (16.58 ± 0.69 pS; Figure 4C) similar to conductance values of 16.53 pS we previously described in the laboratory (Gratacos-Batlle et al. 2014). As expected GluA1:γ2 fusion protein (4-TARPed) responses were increased ~1.4-1.5 fold as previously described when GluA1 was co-transfected together with γ2 (Soto et al. 2014) (16.58 ± 0.69 pS for 0-TARP *vs.* 24.34 ± 1.69 pS for 4-TARP; p=0.0019; n=10 and 16 respectively; Figure 4B-C). Surprisingly, the 2-TARP condition (co-transfection of GluA1 and GluA1:γ2) did not increase single-channel conductance (16.58 ± 0.69 pS for 0-TARP *vs.* 17.03 ± 2.06 pS for 2-TARP; p=0.8373 student's *t*-test; n=10 for both conditions), indicating that 2 TARPs were not sufficient to increase AMPAR conductance.

While it is true that TARPs have a profound effect on single channel conductance of AMPARs (Soto et al. 2007; Soto et al. 2009) their effect on the open probability

250 is more controversial. Some studies have shown an increase of open probability in
251 AMPARs mediated by γ2 (Suzuki et al. 2008) while others have not observed such
252 an increase with γ2 nor with other members of the TARP I subfamily (Soto et al.
253 2009; Shi et al. 2009). The NSFA also allows determination of the number of
254 channels contributing to a given response besides of the unitary conductance.
255 Henceforth, peak open probability ($P_{o,peak}$) can be easily deduced from the
256 experimental mean peak current analysed. We therefore determined the $P_{o,peak}$ of
257 CP-AMPARs when 2 or 4 TARPs were forming part of the complex. As shown in
258 Figure 4D, we did not find any increase of $P_{o,peak}$ regardless of the amount of TARP
259 in the AMPAR complex (0.54 ± 0.06 for 0-TARP *vs.* 0.47 ± 0.06 for 2-TARPs;
260 p=0.3925 student's *t*-test; n=9 and 10 respectively) and (0.54 ± 0.06 *vs.* 0.62 ±
261 0.05 for 4-TARPs; p=0.3691 student's *t*-test; n= 9 and 17 respectively).
262 Additionally, no change between the 2 different stoichiometries was observed (0.47
263 ± 0.06 for 2-TARPs *vs.* 0.62 ± 0.05 for 4-TARPs; p=0.0885 student's *t*-test; n=10
264 and 17 respectively).
265
266 <u>Characterization of GluA4c</u>
267 In order to study the effect of stoichiometry on heteromeric GluA2-containing CI-
268 AMPARs, we focused on GluA2/GluA4, the putative AMPAR present in CGCs
269 (Mosbacher et al. 1994). However, an alternative splicing short isoform of GluA4 –
270 GluA4c – is highly expressed in CGCs (Gallo et al. 1992; Kawahara et al. 2004)
271 and we thus considered that GluA2/GluA4c would be a better readout of CGC
272 AMPARs. Consequently, the examination of this specific combination would permit
273 us to study CI-AMPARs and compare later on the results from expression systems
274 with data extracted from CGCs.
275
276 We first explored the behaviour of homomeric GluA4c(i) (referred hereafter as
277 GluA4c) receptors given the relative scarcity of data with regard to GluA4c in the
278 literature. When both forms of GluA4 were compared we observed that GluA4c
279 homomeric AMPARs were functionally identical to GluA4 homomers. No
280 differences were spotted in the single channel conductance or peak open

281 probability (Figure S1A-B) measured by means of NSFA. Likewise, desensitization
282 kinetics did not differ between both isoforms (Figure S1C). Finally, both homomeric
283 receptors presented the same degree of intracellular block by spermine (Figure
284 S1D-E).
285
286 <u>CI-AMPAR single channel conductance is differentially affected depending on</u>
287 <u>TARP location within AMPAR complex</u>
288 Once GluA4c properties were validated, we created a GluA4c:γ2 fusion protein to
289 study AMPAR/TARP stoichiometry in CI-AMPARs. Unlike homomeric GluA1
290 receptors, in a heteromeric receptor such as GluA2/GluA4c, a 2-TARPed
291 configuration might be achieved by locating the TARPs either in the GluA2 or in
292 GluA4c subunit. Since this might be relevant, we co-transfected GluA2, GluA4c,
293 GluA2:γ2 or GluA4c:γ2 to obtain 0, 2-TARPed in GluA4c, 2-TARPed in GluA2 or a
294 fully TARPed heteromeric AMPARs. We studied responses in out-side out patches
295 where GluA2 presence into the AMPAR was evaluated with the linearity of the
296 responses (Figure 5A).
297
298 NSFA performed on glutamate-evoked responses onto patches from tsA201 cells
299 transfected with different combinations (Figure 5B-C) depicted a remarkable effect
300 not observed with CP-AMPARs. Although any number of TARPs into the CI-
301 AMPAR was sufficient to increase single channel conductance as reported
302 previously (Jackson et al. 2011) ($p<0.001$ for all comparisons between 0-TARPs
303 and the other TARPed groups; Figure 5C-D), the TARP location within the complex
304 was important in determining the extent of conductance increase. Specifically, the
305 TARP γ2 intensified its effect on single channel conductance when it was attached
306 to GluA2 subunit compared with GluA4c (15.85 ± 1.62 pS *vs.* 9.72 ± 1.09 pS for γ2
307 attached to GluA2 or GluA4c respectively; $p<0.01$; student's *t*-test; n=10 and 20
308 patches), which represents a 309% and an 189% of conductance increase respect
309 to GluA2/GluA4c (5.13 ± 0.50 pS). Finally, peak open probability deducted from the
310 same NSFA did not seem to be affected regardless of the number of TARPs or
311 their location on GluA2-containing heteromers (Figure 5E).

312

313 TARP γ2 linked to GluA4c slows down desensitization kinetics of CI-AMPARs

314 The striking observation about a differential modulation of γ2 depending on its
315 particular position into the receptor prompted us to investigate whether other
316 properties of CI-AMPARs were also affected differentially when γ2 was linked to
317 one or another subunit. Figure 6A-B shows that desensitization kinetics of
318 GluA2/GluA4c heteromeric combination (0T) were slowed down only when γ2 was
319 linked to GluA4c subunit irrespective of a 2- or 4-TARP stoichiometry. Indeed, the
320 kinetics of GluA2/GluA4c:γ2 – 2T(A4c) – were not different from
321 GluA2:γ2/GluA4c:γ2 – 4T – (7.23 ± 0.43 ms for 2T(A4c) *vs.* 8.43 ± 0.61 ms for 4T;
322 $p>0.05$; Mann Whitney *U*-test; n=21 and 20 respectively; Figure 6C) while both
323 combinations were slower than 0T or 2T(A2) ($p<0.05$; Figure 6C). Finally, γ2 linked
324 to GluA2 subunits did not seem to affect GluA2/GluA4c desensitization (4.76± 0.28
325 ms for 0T *vs.* 5.42 ± 0.40 ms for 2T(A2); $p>0.05$; student's t-test; n=14 and 11,
326 respectively). Thus, kinetic behaviour in CI-AMPARs is apparently not changed by
327 γ2 unless the TARP is attached to GluA4c subunit. Regarding the activation time to
328 reach the peak current (rise time), we did not notice any variation amongst the
329 different combinations tested (Figure 6D).

330

331 TARP γ2 hinders recovery from desensitization of CI-AMPARs by acting on
332 specific subunits

333 We also checked how recovery from desensitization of CI-AMPARs was affected
334 by distinct AMPAR:TARP stoichiometries. While γ2 enhanced recovery from
335 desensitization from CP-AMPARs in a stoichiometry dependent manner, this was
336 not the case for CI-AMPARs where faster recoveries were not observed regardless
337 of any amount of TARP present into the AMPAR. Interestingly the opposite effect
338 (slowest recovery from desensitization) was observed for the 2T(A2) receptor
339 (Figure 6E-G).

340

341 CI-AMPAR pharmacology is altered depending on their TARP stoichiometry

342 A previous study revealed that AMPAR pharmacology is dependent on the number
343 of TARPs, as the efficiency of the partial agonist kainate is enhanced as the
344 number of TARPs increase into the AMPAR complex (Shi et al. 2009). We
345 wondered whether perampanel, a non-competitive inhibitor of AMPARs, would vary
346 its blocking effect on AMPARs depending on the number of TARPs present. To
347 address this question, we performed recordings where we rapidly applied
348 perampanel in a set of experiments where whole-cell currents were activated in
349 transfected tsA201 held at -60mV with 100 μM AMPA plus 50 μM cyclothiazide to
350 avoid desensitization (Figure S2A). The outcome of those experiments did show
351 the same pattern as the one found for desensitization: TARP γ2 modified the
352 percentage of block only when attached to GluA4c subunit. CI-AMPARs with 2
353 TARPs at the GluA2 subunit displayed a similar block as TARPless CI-AMPARs
354 (47.33 ± 5.95 % for 0T *vs.* 46.13 ± 5.47 % for 2T(A2); $p>0.05$; student's t-test; n= 6
355 and 5, respectively; Figure S2C). However, the block by perampanel in a 2-
356 TARPed at GluA4c (70.65 ± 8.06; n=7) and in a 4-TARPed CI-AMPARs (71.64 ±
357 6.76; n=6) was higher than for TARPless receptors ($p<0.05$ for 0T *vs.* 2T(A4c) and
358 0T *vs.* 4T; student's t-tests).
359
360 <u>Somatic AMPARs from cerebellar granule cells display features of 2-TARPed</u>
361 <u>AMPARs</u>
362 CGCs have a high expression of GluA2 and GluA4c AMPAR subunits. Besides,
363 these neurons only express two members of the TARPs (γ2 and γ7) (Fukaya et al.
364 2005) and no other auxiliary subunits such as cornichons have been described to
365 be functionally present. While γ2 has been proved to be essential in AMPAR
366 signalling in this cell type (Chen et al. 2000), the role of γ7 does not seem to be
367 important to determine CI-AMPAR expression in granule cells (Studniarczyk et al.
368 2013). This converts CGCs into a well-defined system to study AMPARs. Thus, to
369 determine whether CI-AMPARs in CGCs showed properties indicative of a given
370 TARP stoichiometry, we firstly extracted somatic patches from 6-8 days in vitro
371 CGC cultures (Figure 7A) and applied the selective agonist AMPA at 100 μM. We
372 obtained non-rectifying responses such as the one shown in Figure 7B and

373 performed NSFA (Figure 7C-D) to extract single channel conductance and peak
374 open probability values from the recorded responses (Figures 7E-F; orange box)
375 and we also calculated desensitization values from those same patches (Figure
376 7G; orange box). We next compared those results with the ones obtained in
377 expression systems shown previously in figures 5 and 6. Figures 7E to G show, for
378 each analysed parameter, the CGCs results (orange box) together with the
379 different combinations analysed in which dull colours represent the comparable
380 combinations (with no significant differences) and in loose grey the improbable
381 combination responsible for currents found in CGCs ($p<0.05$). Taken together, it
382 was clear that values obtained from CGCs were closely equivalent to values from
383 recombinant receptors only for a 2-TARPed CI-AMPAR with the two TARP
384 molecules linked to the GluA2 subunit.
385
386 We next studied the recovery from desensitization in CGCs and compared the
387 results with the different CI-AMPAR combinations analysed in this study.
388 Surprisingly, we consistently recorded currents with an exceptionally slow recovery
389 that were different from any CI-AMPAR studied (Figure 7I). Given that no other
390 TARP seem to be present on CGCs except γ7, we asked if this auxiliary subunit
391 was responsible for the extraordinary slow recovery seen on AMPARs from CGCs.
392 We examined the presence/absence of γ7 by applying a 20 second jump of AMPA
393 to CGC somatic patches. This type II TARP has been demonstrated to confer a
394 remarkable feature to either homomeric and heteromeric GluA2-containing
395 AMPARs consisting in resensitization of the current a few seconds after
396 desensitization (Kato et al. 2007; Kato et al. 2010). We did not appreciate any
397 change in desensitized current in the presence of the agonist for the whole
398 recording period (Figure 7J) ruling out any contribution of γ7 to CI-AMPAR currents
399 from somatic CGCs. We also wondered about the possibility that the use of the
400 partial agonist (AMPA) to elicit the currents might slow down the recovery from
401 desensitization. However, recordings from cell lines studying GluA2:γ2+GluA4c did
402 not vary when we used AMPA as agonist (data not shown) ruling out this
403 possibility. Considering the reported absence of other members of the TARP

404 family, the functional absence of CNIH2 (Shi et al. 2010) and the really low
405 expression of other AMPAR auxiliary proteins as GSG1L and CKAMP44 (shisa9)
406 (Zeisel et al. 2018) in CGCs, our results suggest that another "unknown player"
407 might be present into the complex, which would be responsible for the extremely
408 low recovery from desensitization. Regardless, our results seem to indicate that CI-
409 AMPARs from somatic CGCs are very possibly modulated by two γ2 molecules
410 attached to the GluA2 subunits.
411
412 **Discussion**
413 One of the first evidences of a functionally variable AMPAR-TARP stoichiometry
414 came from the observation that mEPSCs were differentially altered depending on
415 the TARP expression levels (Milstein et al. 2007). Shortly after, by using fusion
416 constructs similar to the ones used in our study it was seen that the pharmacology
417 – the kainate efficiency – of recombinant AMPARs was stoichiometry-dependent
418 (Shi et al. 2009). This same work suggested that AMPARs from hippocampal
419 pyramidal and dentate gyrus granule neurons were 4 and 2-TARPed, respectively
420 although a 2-TARPed complex was shown to drive AMPAR function at the main
421 AMPAR combination found in hippocampal pyramidal neurons (Herguedas et al.
422 2019). Finally, recently published work has provided evidence for the presence of
423 different stoichiometries in cerebellar cells – 2 and 4 TARPed AMPARs in stellate
424 and Purkinje cells respectively (Dawe et al. 2019). We have expanded these
425 previous findings by carefully dissecting the effect of different stoichiometries on
426 AMPAR basic properties. We demonstrate a sophisticated modulation of TARPs
427 either in CP- and CI-AMPARs and we propose that 2 TARPs acting on the gating-
428 controlling BD "pore distal" subunit GluA2 modulates somatic AMPARs in CGCs in
429 line with recent reports on AMPARs in other neuronal types (Herguedas et al.
430 2019).
431
432 <u>Gradual *vs*. all-or-nothing modulation of AMPARs by TARPs</u>
433 We have found a clear gradual stoichiometry dependence for some of the
434 parameters modulated by TARPs. In example, desensitization kinetics, attenuation

435 of polyamine block by TARPs or recovery from desensitization of GluA1 homomers
436 are differentially altered when 2 or 4 TARPs are part of the AMPAR complex.
437 However, a more intricate modulation appears to be present since a full TARPed
438 GluA1 receptor is necessary to vary other CP-AMPAR intrinsic properties such as
439 single channel conductance or rise time. On the other hand, other characteristics
440 are not altered by the number of TARPs acting on AMPARs (open probability).
441 Thus, a multifaceted scenario arises regarding how TARPs alter AMPAR
442 behaviour. It might be interesting in the future to test whether other auxiliary
443 subunits from the TARP family modulate the AMPAR features studied here,
444 especially single channel conductance since 4 copies of γ2 appear to be required
445 to induce the typical increase of TARPs, which is well described in the literature
446 (Soto et al. 2007; Shi et al. 2009; Soto et al. 2009; Suzuki et al. 2008; Tomita et al.
447 2005) and given that type Ib TARPs (γ4 and γ8) seem to associate with AMPARs
448 in a 2-TARPed dependent manner (Hastie et al. 2013; Herguedas et al. 2019)
449 although they clearly produce an increase in AMPAR channel conductance (Shi et
450 al. 2010; Suzuki et al. 2008; Soto et al. 2009).
451
452 In our hands, AMPAR rise time of the current appears to be slightly affected only
453 with the receptor saturated with four γ2 molecules. For this same type of
454 homomeric CP-AMPAR it has been shown in HEK cells that only TARPs γ4 and γ8
455 are able to increase the period of time to the peak response (Milstein et al. 2007).
456 Since these contradictory results have been obtained in the same type of
457 expression system, the disparity in the outcome might be explained by the fact that
458 in Milstein et al. TARPs and AMPAR subunits were transfected into the cells using
459 two separated plasmids thus raising the possibility that AMPARs studied in the
460 above-mentioned work were not fully saturated with γ2. However, it is interesting
461 that in Milstein's work, γ4 increased the rise time despite the fact that the most
462 prevalent and favoured conformation when γ4 is the auxiliary subunit modulating
463 GluA1 is 2-TARPed (Hastie et al. 2013), showing again the huge difference in the
464 effects that distinct TARPs have on AMPARs. Previous mEPSCs recordings from
465 CGCs, which are mediated by CI-AMPARs have revealed no differences in the rise

466 time of these quantal synaptic currents when the “dose” of TARP γ2 was altered
467 into the receptor by using homozygous or heterozygous stargazer mice (Milstein et
468 al. 2007). In line with these results, our data of rise time of GluA2/GluA4c seems to
469 indicate that AMPAR current activation is independent of the number of TARPs
470 modulating the receptor in CI-AMPARs.
471
472 GluA2 preference of TARP γ2 in native AMPARs
473 Our data from CGCs suggest that, in a GluA2-containing heteromeric AMPAR, γ2
474 preferentially binds to GluA2 subunits to modulate ion channel properties. A very
475 recent publication by Greger’s lab has shown that in GluA1/GluA2 heteromers, the
476 main AMPAR combination present in the hippocampus (Tomita et al. 2003;
477 Schwenk et al. 2014), TARP γ8 binds to GluA2 subunits (Herguedas et al. 2019). It
478 is possible that the 2-TARPed AMPAR arrangement found in this cell type might be
479 determined by the presence of CNIH2 in the AMPARs (Gill et al. 2011; Kato et al.
480 2010). However, in granule cells from the cerebellum CNIH2 functional expression
481 at plasma membrane is absent (Shi et al. 2010) and yet a 2-TARPed stoichiometry
482 seems to be functionally present, indicating also a preferential 2-TARPed
483 disposition at GluA2 in heteromeric GluA2-containing AMPARs. Moreover,
484 structural studies done with γ2 suggest that TARPs preferentially bind to BD “pore
485 distal” subunits (Twomey et al. 2016), a position preferentially occupied by GluA2
486 subunits (He et al. 2016; Herguedas et al. 2019) (but see (Herguedas et al. 2016)).
487 Thus, our results strengthen the idea of a preferential arrangement of TARPs into
488 an heteromeric complex.
489
490 Functional AMPAR/TARP stoichiometry in granule cells from the cerebellum
491 Our experiments indicate that 2-TARPed AMPARs are responsible for somatic
492 responses in CGCs. In fact, the overexpression of TARP γ2 in this cell type
493 increased kainate affinity (Milstein et al. 2007), indicating that CGCs are not totally
494 saturated by TARPs since the efficiency to kainate is strongly dependent on the
495 number of TARPs in the complex (Shi et al. 2009). When comparing the data from
496 GluA2/GluA4 heteromeric receptors using fusion proteins with those form CGCs it

is evident that neither zero TARPs (low conductance) nor four TARPs (slow desensitization kinetics) are modulating somatic AMPARs in CGCs. Importantly, the findings in CGCs closely recapitulated those on expression systems only when 2 TARPs were attached to GluA2 subunit. It has been suggested that TARP subtypes might have different binding sites in the AMPAR complex (Greger et al. 2017) on the basis that for example only two γ4 can co-assemble with AMPARs as seen with single-molecule photobleaching in live cells (Hastie et al. 2013).

In hippocampal CA1 neurons, almost exclusively expressing heteromeric AMPARs (Lu et al. 2009; Wenthold et al. 1996), 2-TARPs stoichiometry – together with 2 CNIHs – has been proven to be present (Gill et al. 2011). This stoichiometry of 2 TARPs and 2 CNIHs molecules assembling with CI-AMPARs might not be possible in CGCs due to the lack of cornichon homolog proteins (Schwenk et al. 2014). However, in CGCs, both γ2 and γ7 are expressed and thus γ7 could potentially be playing a role at somatic AMPARs. This is why we decided to explore resensitization in CGC somatic patches – a slow recovery of steady-state current after desensitization upon a prolonged agonist application firstly shown to be dependent on γ7 (Kato et al. 2007). Apart from γ7, also γ4 and γ8 show this exceptional resensitization signature (Gill et al. 2011) (but see (Carbone and Plested, 2016)). In the cerebellum the expression of γ4 and γ8 is negligible (Tomita et al. 2003) and CGCs do not express these TARPs (Fukaya et al. 2005). Besides, γ7 has been shown to selectively suppress CI-AMPARs in CGCs and its functional expression would be restricted to synaptic CP-AMPARs (Studniarczyk et al. 2013) although γ7 has been suggested not to have an important involvement in excitatory transmission in granule cells (Yamazaki et al. 2015). Our recordings from somatic patches of CGCs did not show the typical increase in steady-state current upon a 30 seconds in the presence of the full agonist AMPA, indicating that probably no functional γ7 molecules are present in somatic CI-AMPARs form CGCs in accordance with the poor role of this atypical TARP in granule neurons physiology shown to date (Studniarczyk et al. 2013; Yamazaki et al. 2015).

528 Another reason to explore resensitization in CGCs is that this property is a
529 potential way to discriminate for a fully TARPed AMPAR since it has been
530 suggested that resensitization is a fingerprint that indicates the presence of 4-
531 TARPed AMPARs (Kato et al. 2010). Indeed, Purkinje cells from stargazer mice,
532 with low γ7 stoichiometry lack this feature (Gill et al. 2011), indicating that
533 saturation of TARPs is indispensable to present resensitization. The absence of
534 resensitization in CGCs thus might be indicative of a 2-TARPed conformation.
535 Despite recent reports showing new evidence that resensitization might not be a
536 unique feature of TARPs γ4, γ7 and γ8 (Carbone and Plested, 2016), this does not
537 exclude the possibility that resensitization is a characteristic signature of a fully
538 TARPed receptor, thus reinforcing our conclusion of a 2-TARPed GluA2/GluA4c
539 receptor in CGCs.
540
541 The results from different AMPAR-TARP combinations in recombinant systems
542 showed that the 2-TARP-GluA2 condition displayed the slowest recovery from
543 desensitization. AMPARs from somatic CGCs did show an even slower recovery
544 rate compared with our expression systems data. We ruled out the possibility that
545 the agonist used elicited a change in recovery kinetics (data not shown). One
546 possibility of such slowdown in the recovery could be the presence of an
547 "unknown" protein attached to the complex modulating the native AMPAR. In this
548 regard, recovery from desensitization is strongly decreased either in neurons and
549 heteromeric recombinant AMPARs when they are co-expressed with other auxiliary
550 subunits of the CKAMP family as CKAMP39 (Farrow et al. 2015), CKAMP44 (von
551 Engelhardt et al. 2010) or CKAMP52 (Klaassen et al. 20116) (*but see* (Farrow et
552 al. 2015)). Interestingly, both CKAMP39 and 52 are highly expressed in the
553 cerebellum (Farrow et al. 2015; Klaassen et al. 2016). Future work will elucidate
554 whether apart from two γ2 molecules, CKAMPs play a role in AMPAR properties in
555 CGCs.
556
557 A possible flaw in our study comes from the fact that in order to study AMPAR
558 currents in CGCs, we have used the specific agonist AMPA to circumvent the

559 stimulation of other glutamate-activated receptors – specially the kainate receptors
560 present in CGCs (Bahn et al. 1994; Belcher and Howe, 1997). Certainly, the use of
561 AMPA *vs.* glutamate may potentially alter the output values. When we checked for
562 agonist variation on GluA4c with both agonists, neither weighted single-channel
563 conductance nor open probability changed (data not shown). Previously,
564 differences in channel conductance estimates have been described when using
565 Kainate *vs.* AMPA to activate AMPARs (Jonas and Sakmann 1992; Swanson et al.
566 1997) but subconductance levels of CP-AMPARs have been shown to have similar
567 values regardless of the use of AMPA or glutamate as agonist (Swanson et al.
568 1997). Furthermore, for GluA2/GluA4 similar conductance values have been
569 described for both agonists 5.5-6 pS (Swanson et al. 1997), which match the ones
570 observed in this and other studies (Jackson et al. 2011) using the agonist
571 glutamate. Conversely, in our hands, AMPAR desensitization kinetics of GluA4c
572 seemed to be significantly slower when AMPA was used as agonist (data not
573 shown) despite the findings in previous reports that the kinetic properties of AMPA-
574 activated GluA4 homomers were comparable to those activated by glutamate
575 (Swanson et al. 1997). In principle, this might confuse the interpretation when
576 comparing recordings in expression systems (glutamate used as agonist) with
577 neurons (AMPA used as agonist). However, the kinetics of currents evoked with
578 AMPA in CGCs were fast – indeed as rapid as the quicker responses observed in
579 expression systems with glutamate. Therefore, it would be expected that the
580 AMPAR-mediated responses in CGCs using the glutamate agonist would be faster
581 than using AMPA as agonist– in any case kinetics would be overestimated – which
582 still rules out that the possible stoichiometry present in CGCs were any of the slow
583 combinations: 4 TARPs or 2 TARPs attached to GluA4c.
584
585 <u>Final remarks</u>
586 AMPAR responses reckon on their subunit composition but also importantly rely on
587 the type of auxiliary subunit/s accompanying them. This work adds important
588 information on the extraordinary degree of functional variety in AMPARs by
589 showing that AMPAR properties can be modulated differently depending on the

590 number of TARPs, the type of AMPAR and the specific interactions that these
591 auxiliary subunits set up with given GluAs. The broad number of possible
592 combinations of pore-forming plus auxiliary subunits and stoichiometries that can
593 be achieved on AMPARs generate a profuse diversity in glutamatergic responses
594 in the brain. One of the major challenges scientists of the field will face is to resolve
595 the exact composition of the AMPAR complex at different neurons.
596
597 **Methods**
598 Cell lines culture and transfection
599 tsA201 cells were used for electrophysiological experiments and were maintained
600 and transfected with several constructs as described in (Gratacos-Batlle et al.
601 2014). More detailed information is available on Supplementary Information
602 (Supplementary File 1).
603
604 Cerebellar granule cells (CGCs) culture
605 Primary cultures of CGCs were prepared from pups on postnatal day 7–8 as
606 previously described (Verdaguer et al. 2002). The cerebella from 8 to 10 mice pups
607 were collected in 9.5 ml buffer containing 120 mM NaCl, 5 mM KCl, 25 mM
608 HEPES, and 9.1 mM glucose. Thereafter, meninges were carefully removed and
609 cerebella were dissected out, minced carefully with a blade, and dissociated at
610 37°C for 15 min with a solution containing 250 µg /ml trypsin. After 15 minutes,
611 solution with 2.7 µg/ml DNAse and 8.32 µg/ml soybean trypsin Inhibitor (SBTI) was
612 added. CGCs were separated from non-dissociated tissue by sedimentation and,
613 finally, resuspended in basal medium Eagle's (BME) supplemented with 10%
614 inactivated fetal calf serum, 25 mM KCl, and gentamicin (5mg/ml), and plated onto
615 poly-L-lysine-coated 24-well plates at a density of 300,000 cells/cm^2. After 16–19h
616 in culture, cytosine arabinoside was added to a final concentration of 10 µM to
617 inhibit glial cell proliferation. Electrophysiological experiments were performed at 6
618 to 8 days after platting.
619
620 Basic electrophysiological procedures

621 Recordings were performed from isolated transfected cells or cerebellar granule
622 cells (CGCs) visualized with an inverted epifluorescence microscope (Axio-Vert.A1;
623 Zeiss). Cells expressing EGFP and/or mCherry fluorescent proteins were selected
624 for patch-clamp recordings. Macroscopic currents were recorded at room
625 temperature (22-25ºC) from outside-out membrane patches or from isolated whole
626 cells using an Axopatch 200B amplifier and acquired using a Digidata 1440A
627 interface board and pClamp 10 software (Molecular Devices Corporation,
628 Sunnyvale, CA).
629
630 For all recordings the extracellular solution contained (in mM):145 NaCl, 2.5 KCl, 1
631 $CaCl_2$, 1 $MgCl_2$, 10 glucose and 10 HEPES (pH to 7.42 with NaOH). The
632 extracellular control solution applied with the fast agonist application tool was
633 composed by extracellular solution diluted 4% with miliQ H_2O. The extracellular
634 agonist solution applied with the fast agonist application tool was extracellular
635 solution plus 2.5 mg/ml of sucrose with 10 mM glutamate for tsA201 recordings or
636 100 μM AMPA for tsA201 cells and CGC recordings. The intracellular pipette
637 solution contained (in mM): 145 CsCl, 2.5 NaCl, 1 Cs-EGTA, 4 MgATP, and 10
638 HEPES (pH to 7.2 with CsOH). The polyamine spermine tetrahydrochloride
639 (Sigma-Aldrich) was added to intracellular solution at 100 μM in all cases, which
640 has been calculated to yield free concentrations in the physiological range (Soto et
641 al. 2007).
642
643 Patch pipettes were fabricated from borosilicate glass (1.5 mm o.d. and 0.86 mm
644 i.d.; Harvard Apparatus, Edenbridge, UK) by using a Horizontal puller (Sutter P-97)
645 with several resistances depending on the configuration used.
646
647 Recordings were performed in the whole-cell or outside-out configurations, where
648 different parameters as recovery from desensitization, desensitization kinetics,
649 single channel conductance, peak open probability, intracellular polyamine block or
650 percentage of block by non-competitive antagonists was tested as explained in
651 detail in Supplementary File 1.

652

653 Statistical Analysis

654 Analysis of current waveforms and curve fitting was performed with IGOR Pro 6.06
655 (Wavemetrics) using NeuroMatic 2.03 ((Rothman and Silver, 2018);
656 http://www.neuromatic.thinkrandom.com). Statistical analysis was performed using
657 GraphPad Prism version 8.0.1 for Mac OS X (GraphPad Software, San Diego
658 California USA, www.graphpad.com). Comparisons between two groups were
659 performed using the parametric Student' *t*-test for data following a normal
660 distribution or using the non-parametric Mann-Whitney U test for comparisons
661 between groups in which one of them did not follow a normal distribution.
662 Differences were considered significant as follows: *$p < 0.05$, **$p<0.01$, ***$p<0.001$
663 and ****$p<0.0001$.

664

665 Extended methodology is available in Supplementary File 1 (Animals and housing,
666 constructs, electrophysiological configurations used and analysis performed).

667

668 **References**

669 Bahn, S., Volk, B., and Wisden, W. (1994). Kainate receptor gene expression in
670 the developing rat brain. J Neurosci *14*, 5525-5547.
671 Belcher, S.M., and Howe, J.R. (1997). Characterization of RNA editing of the
672 glutamate-receptor subunits GluR5 and GluR6 in granule cells during
673 cerebellar development. Brain Res Mol Brain Res *52*, 130-138.
674 Bowie, D., and Mayer, M.L. (1995). Inward rectification of both AMPA and kainate
675 subtype glutamate receptors generated by polyamine-mediated ion channel
676 block. Neuron *15*, 453-462.
677 Burnashev, N., Monyer, H., Seeburg, P.H., and Sakmann, B. (1992). Divalent ion
678 permeability of AMPA receptor channels is dominated by the edited form of a
679 single subunit. Neuron *8*, 189-198.
680 Cais, O., Herguedas, B., Krol, K., Cull-Candy, S.G., Farrant, M., and Greger, I.H.
681 (2014). Mapping the interaction sites between AMPA receptors and TARPs
682 reveals a role for the receptor N-terminal domain in channel gating. Cell Rep *9*,
683 728-740.
684 Carbone, A.L., and Plested, A.J. (2016). Superactivation of AMPA receptors by
685 auxiliary proteins. Nat Commun *7*, 10178.
686 Chen, L., Chetkovich, D.M., Petralia, R.S., Sweeney, N.T., Kawasaki, Y.,
687 Wenthold, R.J., Bredt, D.S., and Nicoll, R.A. (2000). Stargazin regulates
688 synaptic targeting of AMPA receptors by two distinct mechanisms. Nature *408*,
689 936-943.
690 Dawe, G.B., Kadir, M.F., Venskutonytė, R., Perozzo, A.M., Yan, Y., Alexander,
691 R.P.D., Navarrete, C., Santander, E.A., Arsenault, M., Fuentes, C.*, et al.*
692 (2019). Nanoscale Mobility of the Apo State and TARP Stoichiometry Dictate
693 the Gating Behavior of Alternatively Spliced AMPA Receptors. Neuron *102*,
694 976-992.e975.
695 Farrow, P., Khodosevich, K., Sapir, Y., Schulmann, A., Aslam, M., Stern-Bach, Y.,
696 Monyer, H., and von Engelhardt, J. (2015). Auxiliary subunits of the CKAMP
697 family differentially modulate AMPA receptor properties. Elife *4*, e09693.
698 Fukaya, M., Yamazaki, M., Sakimura, K., and Watanabe, M. (2005). Spatial
699 diversity in gene expression for VDCCgamma subunit family in developing and
700 adult mouse brains. Neurosci Res *53*, 376-383.
701 Geiger, J.R., Melcher, T., Koh, D.S., Sakmann, B., Seeburg, P.H., Jonas, P., and
702 Monyer, H. (1995). Relative abundance of subunit mRNAs determines gating
703 and Ca2+ permeability of AMPA receptors in principal neurons and
704 interneurons in rat CNS. Neuron *15*, 193-204.
705 Gill, M.B., Kato, A.S., Roberts, M.F., Yu, H., Wang, H., Tomita, S., and Bredt, D.S.
706 (2011). Cornichon-2 modulates AMPA receptor-transmembrane AMPA
707 receptor regulatory protein assembly to dictate gating and pharmacology. J
708 Neurosci *31*, 6928-6938.
709 Gill, M.B., Kato, A.S., Wang, H., and Bredt, D.S. (2012). AMPA receptor
710 modulation by cornichon-2 dictated by transmembrane AMPA receptor
711 regulatory protein isoform. Eur J Neurosci *35*, 182-194.

712 Gratacos-Batlle, E., Yefimenko, N., Cascos-Garcia, H., and Soto, D. (2014).
713 AMPAR interacting protein CPT1C enhances surface expression of GluA1-
714 containing receptors. Frontiers in cellular neuroscience *8*, 469-469.
715 Greger, I.H., Khatri, L., Kong, X., and Ziff, E.B. (2003). AMPA receptor
716 tetramerization is mediated by Q/R editing. Neuron *40*, 763-774.
717 Greger, I.H., Watson, J.F., and Cull-Candy, S.G. (2017). Structural and Functional
718 Architecture of AMPA-Type Glutamate Receptors and Their Auxiliary Proteins.
719 Neuron *94*, 713-730.
720 Haering, S.C., Tapken, D., Pahl, S., and Hollmann, M. (2014). Auxiliary subunits:
721 shepherding AMPA receptors to the plasma membrane. Membranes (Basel) *4*,
722 469-490.
723 Hastie, P., Ulbrich, M.H., Wang, H.L., Arant, R.J., Lau, A.G., Zhang, Z., Isacoff,
724 E.Y., and Chen, L. (2013). AMPA receptor/TARP stoichiometry visualized by
725 single-molecule subunit counting. Proc Natl Acad Sci U S A *110*, 5163-5168.
726 He, X.Y., Li, Y.J., Kalyanaraman, C., Qiu, L.L., Chen, C., Xiao, Q., Liu, W.X.,
727 Zhang, W., Yang, J.J., Chen, G.*, et al.* (2016). GluA1 signal peptide
728 determines the spatial assembly of heteromeric AMPA receptors. Proc Natl
729 Acad Sci U S A *113*, E5645-5654.
730 Herguedas, B., García-Nafría, J., Cais, O., Fernández-Leiro, R., Krieger, J., Ho, H.,
731 and Greger, I.H. (2016). Structure and organization of heteromeric AMPA-type
732 glutamate receptors. Science *352*, aad3873.
733 Herguedas, B., Watson, J.F., Ho, H., Cais, O., García-Nafría, J., and Greger, I.H.
734 (2019). Architecture of the heteromeric GluA1/2 AMPA receptor in complex
735 with the auxiliary subunit TARP γ8. Science *364*.
736 Hollmann, M., Hartley, M., and Heinemann, S. (1991). Ca2+ permeability of KA-
737 AMPA--gated glutamate receptor channels depends on subunit composition.
738 Science *252*, 851-853.
739 Jackson, A.C., Milstein, A.D., Soto, D., Farrant, M., Cull-Candy, S.G., and Nicoll,
740 R.A. (2011). Probing TARP modulation of AMPA receptor conductance with
741 polyamine toxins. J Neurosci *31*, 7511-7520.
742 Jackson, A.C., and Nicoll, R.A. (2011). The expanding social network of ionotropic
743 glutamate receptors: TARPs and other transmembrane auxiliary subunits.
744 Neuron *70*, 178-199.
745 Jonas, P., and Sakmann, B. (1992). Glutamate receptor channels in isolated
746 patches from CA1 and CA3 pyramidal cells of rat hippocampal slices. J Physiol
747 *455*, 143-171.
748 Kamboj, S.K., Swanson, G.T., and Cull-Candy, S.G. (1995). Intracellular spermine
749 confers rectification on rat calcium-permeable AMPA and kainate receptors. J
750 Physiol *486 (Pt 2)*, 297-303.
751 Kato, A.S., Gill, M.B., Ho, M.T., Yu, H., Tu, Y., Siuda, E.R., Wang, H., Qian, Y.W.,
752 Nisenbaum, E.S., Tomita, S.*, et al.* (2010). Hippocampal AMPA receptor gating
753 controlled by both TARP and cornichon proteins. Neuron *68*, 1082-1096.
754 Kato, A.S., Zhou, W., Milstein, A.D., Knierman, M.D., Siuda, E.R., Dotzlaf, J.E., Yu,
755 H., Hale, J.E., Nisenbaum, E.S., Nicoll, R.A.*, et al.* (2007). New
756 transmembrane AMPA receptor regulatory protein isoform, gamma-7,
757 differentially regulates AMPA receptors. J Neurosci *27*, 4969-4977.

758 Kawahara, Y., Ito, K., Sun, H., Ito, M., Kanazawa, I., and Kwak, S. (2004). GluR4c,
759 an alternative splicing isoform of GluR4, is abundantly expressed in the adult
760 human brain. Brain Res Mol Brain Res *127*, 150-155.
761 Kawahara, Y., Ito, K., Sun, H., Kanazawa, I., and Kwak, S. (2003). Low editing
762 efficiency of GluR2 mRNA is associated with a low relative abundance of
763 ADAR2 mRNA in white matter of normal human brain. Eur J Neurosci *18*, 23-
764 33.
765 Klaassen, R.V., Stroeder, J., Coussen, F., Hafner, A.S., Petersen, J.D., Renancio,
766 C., Schmitz, L.J., Normand, E., Lodder, J.C., Rotaru, D.C.*, et al.* (2016).
767 Shisa6 traps AMPA receptors at postsynaptic sites and prevents their
768 desensitization during synaptic activity. Nat Commun *7*, 10682.
769 Koh, D.S., Burnashev, N., and Jonas, P. (1995). Block of native Ca(2+)-permeable
770 AMPA receptors in rat brain by intracellular polyamines generates double
771 rectification. J Physiol *486 (Pt 2)*, 305-312.
772 Kott, S., Werner, M., Körber, C., and Hollmann, M. (2007). Electrophysiological
773 properties of AMPA receptors are differentially modulated depending on the
774 associated member of the TARP family. J Neurosci *27*, 3780-3789.
775 Louros, S.R., Caldeira, G.L., and Carvalho, A.L. (2018). Stargazin
776 Dephosphorylation Mediates Homeostatic Synaptic Downscaling of Excitatory
777 Synapses. Front Mol Neurosci *11*, 328.
778 Louros, S.R., Hooks, B.M., Litvina, L., Carvalho, A.L., and Chen, C. (2014). A role
779 for stargazin in experience-dependent plasticity. Cell Rep *7*, 1614-1625.
780 Lu, W., Shi, Y., Jackson, A.C., Bjorgan, K., During, M.J., Sprengel, R., Seeburg,
781 P.H., and Nicoll, R.A. (2009). Subunit composition of synaptic AMPA receptors
782 revealed by a single-cell genetic approach. Neuron *62*, 254-268.
783 Milstein, A.D., Zhou, W., Karimzadegan, S., Bredt, D.S., and Nicoll, R.A. (2007).
784 TARP subtypes differentially and dose-dependently control synaptic AMPA
785 receptor gating. Neuron *55*, 905-918.
786 Mosbacher, J., Schoepfer, R., Monyer, H., Burnashev, N., Seeburg, P.H., and
787 Ruppersberg, J.P. (1994). A molecular determinant for submillisecond
788 desensitization in glutamate receptors. Science *266*, 1059-1062.
789 Payne, H.L. (2008). The role of transmembrane AMPA receptor regulatory proteins
790 (TARPs) in neurotransmission and receptor trafficking (Review). Mol Membr
791 Biol *25*, 353-362.
792 Priel, A., Kolleker, A., Ayalon, G., Gillor, M., Osten, P., and Stern-Bach, Y. (2005).
793 Stargazin reduces desensitization and slows deactivation of the AMPA-type
794 glutamate receptors. J Neurosci *25*, 2682-2686.
795 Rothman, J.S., and Silver, R.A. (2018). NeuroMatic: An Integrated Open-Source
796 Software Toolkit for Acquisition, Analysis and Simulation of
797 Electrophysiological Data. Front Neuroinform *12*, 14.
798 Rouach, N., Byrd, K., Petralia, R.S., Elias, G.M., Adesnik, H., Tomita, S.,
799 Karimzadegan, S., Kealey, C., Bredt, D.S., and Nicoll, R.A. (2005). TARP
800 gamma-8 controls hippocampal AMPA receptor number, distribution and
801 synaptic plasticity. Nat Neurosci *8*, 1525-1533.
802 Schwenk, J., Baehrens, D., Haupt, A., Bildl, W., Boudkkazi, S., Roeper, J., Fakler,
803 B., and Schulte, U. (2014). Regional diversity and developmental dynamics of
804 the AMPA-receptor proteome in the mammalian brain. Neuron *84*, 41-54.

805 Schwenk, J., Harmel, N., Zolles, G., Bildl, W., Kulik, A., Heimrich, B., Chisaka, O.,
806 Jonas, P., Schulte, U., Fakler, B.*, et al.* (2009). Functional proteomics identify
807 cornichon proteins as auxiliary subunits of AMPA receptors. Science *323*,
808 1313-1319.
809 Shi, Y., Lu, W., Milstein, A.D., and Nicoll, R.A. (2009). The stoichiometry of AMPA
810 receptors and TARPs varies by neuronal cell type. Neuron *62*, 633-640.
811 Shi, Y., Suh, Y.H., Milstein, A.D., Isozaki, K., Schmid, S.M., Roche, K.W., and
812 Nicoll, R.A. (2010). Functional comparison of the effects of TARPs and
813 cornichons on AMPA receptor trafficking and gating. Proc Natl Acad Sci U S A
814 *107*, 16315-16319.
815 Soto, D., Coombs, I.D., Gratacos-Batlle, E., Farrant, M., and Cull-Candy, S.G.
816 (2014). Molecular Mechanisms Contributing to TARP Regulation of Channel
817 Conductance and Polyamine Block of Calcium-Permeable AMPA Receptors.
818 Journal of Neuroscience *34*, 11673-11683.
819 Soto, D., Coombs, I.D., Kelly, L., Farrant, M., and Cull-Candy, S.G. (2007).
820 Stargazin attenuates intracellular polyamine block of calcium-permeable AMPA
821 receptors. Nat Neurosci *10*, 1260-1267.
822 Soto, D., Coombs, I.D., Renzi, M., Zonouzi, M., Farrant, M., and Cull-Candy, S.G.
823 (2009). Selective regulation of long-form calcium-permeable AMPA receptors
824 by an atypical TARP, gamma-5. Nat Neurosci *12*, 277-285.
825 Straub, C., and Tomita, S. (2012). The regulation of glutamate receptor trafficking
826 and function by TARPs and other transmembrane auxiliary subunits. Curr Opin
827 Neurobiol *22*, 488-495.
828 Studniarczyk, D., Coombs, I., Cull-Candy, S.G., and Farrant, M. (2013). TARP γ-7
829 selectively enhances synaptic expression of calcium-permeable AMPARs. Nat
830 Neurosci *16*, 1266-1274.
831 Sullivan, S.J., Farrant, M., and Cull-Candy, S.G. (2017). TARP γ-2 Is Required for
832 Inflammation-Associated AMPA Receptor Plasticity within Lamina II of the
833 Spinal Cord Dorsal Horn. J Neurosci *37*, 6007-6020.
834 Suzuki, E., Kessler, M., and Arai, A.C. (2008). The fast kinetics of AMPA GluR3
835 receptors is selectively modulated by the TARPs gamma 4 and gamma 8. Mol
836 Cell Neurosci *38*, 117-123.
837 Swanson, G.T., Kamboj, S.K., and Cull-Candy, S.G. (1997). Single-channel
838 properties of recombinant AMPA receptors depend on RNA editing, splice
839 variation, and subunit composition. J Neurosci *17*, 58-69.
840 Tomita, S., Adesnik, H., Sekiguchi, M., Zhang, W., Wada, K., Howe, J.R., Nicoll,
841 R.A., and Bredt, D.S. (2005). Stargazin modulates AMPA receptor gating and
842 trafficking by distinct domains. Nature *435*, 1052-1058.
843 Tomita, S., Chen, L., Kawasaki, Y., Petralia, R.S., Wenthold, R.J., Nicoll, R.A., and
844 Bredt, D.S. (2003). Functional studies and distribution define a family of
845 transmembrane AMPA receptor regulatory proteins. J Cell Biol *161*, 805-816.
846 Traynelis, S.F., Wollmuth, L.P., McBain, C.J., Menniti, F.S., Vance, K.M., Ogden,
847 K.K., Hansen, K.B., Yuan, H., Myers, S.J., and Dingledine, R. (2010).
848 Glutamate receptor ion channels: structure, regulation, and function.
849 Pharmacol Rev *62*, 405-496.

850 Turetsky, D., Garringer, E., and Patneau, D.K. (2005). Stargazin modulates native
851 AMPA receptor functional properties by two distinct mechanisms. J Neurosci
852 *25*, 7438-7448.
853 Twomey, E.C., Yelshanskaya, M.V., Grassucci, R.A., Frank, J., and Sobolevsky,
854 A.I. (2016). Elucidation of AMPA receptor-stargazin complexes by cryo-
855 electron microscopy. Science *353*, 83-86.
856 Verdaguer, E., García-Jordà, E., Jiménez, A., Stranges, A., Sureda, F.X.,
857 Canudas, A.M., Escubedo, E., Camarasa, J., Pallàs, M., and Camins, A.
858 (2002). Kainic acid-induced neuronal cell death in cerebellar granule cells is
859 not prevented by caspase inhibitors. Br J Pharmacol *135*, 1297-1307.
860 von Engelhardt, J., Mack, V., Sprengel, R., Kavenstock, N., Li, K.W., Stern-Bach,
861 Y., Smit, A.B., Seeburg, P.H., and Monyer, H. (2010). CKAMP44: a brain-
862 specific protein attenuating short-term synaptic plasticity in the dentate gyrus.
863 Science *327*, 1518-1522.
864 Wenthold, R.J., Petralia, R.S., Blahos J, I.I., and Niedzielski, A.S. (1996). Evidence
865 for multiple AMPA receptor complexes in hippocampal CA1/CA2 neurons. J
866 Neurosci *16*, 1982-1989.
867 Yamazaki, M., Le Pichon, C.E., Jackson, A.C., Cerpas, M., Sakimura, K., Scearce-
868 Levie, K., and Nicoll, R.A. (2015). Relative contribution of TARPs γ-2 and γ-7
869 to cerebellar excitatory synaptic transmission and motor behavior. Proc Natl
870 Acad Sci U S A *112*, E371-379.
871 Zeisel, A., Hochgerner, H., Lönnerberg, P., Johnsson, A., Memic, F., van der
872 Zwan, J., Häring, M., Braun, E., Borm, L.E., La Manno, G.*, et al.* (2018).
873 Molecular Architecture of the Mouse Nervous System. Cell *174*, 999-
874 1014.e1022.
875

876 **Figure legends**

877

878 **Figure 1.** CP-AMPAR kinetics are differentially affected by AMPAR-TARP
879 stoichiometry.
880 **A.** Traces evoked at -60 mV by rapid application of 10 mM glutamate to outside-out
881 patches from cells expressing GluA1 alone (black; average of 39 responses) or
882 together with 2 (blue; average of 37 responses) or 4 (red; average of 67
883 responses) γ2 subunits. **B**. Pooled data of the weighted time constant of
884 desensitization ($\tau_{w,\ des}$). Box-and-whisker plots indicate the median value (gray
885 line), the 25–75th percentiles (box), and the 10–90th percentiles (whiskers);
886 crosses and filled opened circles represent mean and the individual experimental
887 values respectively (**p<0.01, ***p<0.001, ****p<0.0001). **C**. Pooled data showing
888 the increase in the steady state current only in 4 TARPed CP-AMPARs (**p<0.01,
889 ****p<0.0001). **D**. Rise time of glutamate-activated currents is only affected in a full
890 TARPed CP-AMPAR (*p<0.05).
891 The data from this figure containing statistical tests applied, exact sample number,
892 p values and details of replicates are available in “Figure 1 - Source Data 1”.

893

894 **Figure 2.** Recovery from desensitization of CP-AMPARs is gradually enhanced
895 with increased TARP molecules.
896 **A**. Representative traces of a two-pulse protocol with increasing time interval
897 between pulses for CP-AMPAR without TARPs (GluA1 homomers; black), with 2
898 TARPs (blue) and with 4 TARPs (red). **B**. Recovery from desensitization dynamics
899 where it can be observed the gradual diminishment in the time needed to recover
900 as the TARP dosage increases. **C**. Recovery time constant values for the
901 experiments showed in A and B (**p<0.01, ****p<0.0001).
902 The data from this figure containing statistical tests applied, exact sample number,
903 p values and details of replicates are available in “Figure 2 - Source Data 2”.

904

905 **Figure 3.** CP-AMPAR polyamine block attenuation is dependent on TARP dosage.

A. Representative glutamate-evoked currents from outside-out patches at different membrane potentials from -80 to +80 in 20 mV increments from cells expressing CP-AMPARs, GluA1 (black), GluA1+GluA1: γ2 (blue) and GluA1: γ2 (red). Bottom: Traces at +60 mV and -60mV membrane potentials are marked. **B**. I-V relationships constructed from glutamate-evoked peak currents of patches held at different membrane potentials in different AMPAR-TARP stoichiometries. **B**. Pooled data showing an increase in the RI as the number of TARPs per CP-AMPAR increases. The RI in 2 (blue) and 4 (red, 4 TARPed) TARPs per CP-AMPAR complex is higher compared with 0 TARPs (white, TARPless) (****$p<0.0001$). Box-and-whiskers plots meaning as in Figure 1.
The data from this figure containing statistical tests applied, exact sample number, p values and details of replicates are available in “Figure 3 - Source Data 3”.

Figure 4. Four TARPs are required to increase CP-AMPAR channel conductance.
A. Typical responses at a holding potential of -60 mV to rapid application of 10 mM glutamate to excised patches from cells expressing homomeric GluA1 alone (black; average of 84 responses) or together with 2 (blue; average of 91 responses) or 4 (red; average of 223 responses) γ2 subunits. A single trace is shown in gray overlaid with the mean response. **B**. Current-variance plots for the traces shown in A, the slope of which gave the weighted single-channel conductance. Broken lines show the baseline variance and error bars denote SEM. Single channel conductance values for these recordings are presented. **C**. Pooled data showing an increase of the single channel conductance only in a full-TARPed CP-AMPAR (*$p<0.05$, **$p<0.01$). **D**. Pooled data for peak open probability of CP-AMPARs. The data from this figure containing statistical tests applied, exact sample number, p values and details of replicates are available in “Figure 4 - Source Data 4”.

Figure 5. Single channel conductance of CI-AMPARs is modulated differently by TARPs depending on their location within the complex.

936 **A**. Evoked currents by rapid application of 10 mM glutamate from membrane
937 patches at +60 mV (upward traces) and -60 mV (downward traces) with their
938 corresponding RI. The experimental conditions are designated as grey for 0
939 TARPs per AMPAR, blue for 2 TARPs per AMPAR with γ2 linked to GluA4c, purple
940 for 2 TARPs per AMPAR with γ2 linked to GluA2 and red for 4 TARPs per AMPAR.
941 **B**. Average traces of current responses evoked at -60 mV used for NSNA shown in
942 black overlaid with a representative single response. Insets shown the studied
943 combination. **C**. Current-variance plots for the recordings shown in B, with the
944 weighted single-channel conductance for the single recordings. **D**. Pooled data
945 showing a distinct degree in single channel conductance increase when γ2 is
946 present into the AMPAR complex (*p<0.05, **p<0.01, ***p<0.001, ****p<0.0001). **E**.
947 Pooled data for peak open probability of CI-AMPARs, where no effect of TARP
948 stoichiometry was evident (p>0.05).
949 The data from this figure containing statistical tests applied, exact sample number,
950 p values and details of replicates are available in "Figure 5 - Source Data 5".
951
952 **Figure 6.** CI-AMPAR kinetics differ upon γ2 attachment to GluA4c or GluA2
953 subunit.
954 **A**. Representative traces of currents at -60 mV from cells expressing CI-AMPARs
955 without or with TARP γ2 linked to GluA subunits. Under the traces a scheme of the
956 subunits forming the receptors with γ2 associated to different AMPAR subunits is
957 shown. **B**. Peak-scaled normalization from traces shown in A for a better
958 comparison of desensitization kinetics. **C**. Weighted time constant of
959 desensitization ($\tau_{w,des}$) were is clear that desensitization is slowed only when γ2 is
960 linked to GluA4c subunit (*p<0.05, ***p<0.001, ****p<0.0001).. **D**. Rise time of the
961 current activation is not changed by the AMPAR-TARP stoichiometry. **E.**
962 Representative traces monitoring recovery from desensitization for CI-AMPAR in
963 cells expressing 0 TARPs or 2 TARPs linked to GluA2 subunit where it is manifest
964 the difference between the two conditions. Dashed red line: exponential fitting for
965 the desensitization recovery. **F**. Recovery of desensitization kinetics showing a
966 relatively slow recovery only in 2-TARPed (located in GluA2) CI-AMPARs. **G**.

967 Recovery time constant values for the experiments showed in E and F (**p<0.01,
968 ***p<0.001, ****p<0.0001).
969 The data from this figure containing statistical tests applied, exact sample number,
970 p values and details of replicates are available in “Figure 6 - Source Data 6”.
971
972 **Figure 7.** Somatic currents from CGCs exhibit properties of GluA2:γ2 + GluA4c CI-
973 AMPARs.
974 **A**. CGCs in culture after 7 days in vitro. **B**. Traces at +60mV and -60mV evoked
975 with 100 μM AMPA from a CGC somatic patch showing the typical lineal response
976 of a CI-AMPAR. **C**. Representative response of current evoked at -60 mV by rapid
977 application of 100 μM AMPA to somatic patches from CGCs. Grey: representative
978 single response; black: average of 275 stable responses. **D**. NSFA from the
979 recording in C. **E**. Data showing comparison of single channel conductance values
980 obtained in CGCs (orange box) with recordings from transfected cell lines. The
981 conductance values obtained resembled (without significant difference) to the ones
982 seen with 2T (A2) or 4T conditions (marked in bold grey). **F**. Comparison of peak
983 open probability values from CGCs were only significantly different from recordings
984 in cell lines with 4 TARPs. **G**. Compared data of desensitization time constant (ms)
985 from CGCs with recordings in tsA201 cells. The results are no significantly different
986 from conditions with 0T or 2T(A2). **H**. Representative trace from two-pulse protocol
987 monitoring recovery from desensitization for CGCs somatic patches to 100 μM
988 AMPA application. **I**. Recovery from desensitization kinetics of CGS somatic
989 AMPARs. **J**. Representative response to a 100 μM AMPA application for 20
990 seconds in a somatic patch from CGCs to test for the presence of γ7. No re-
991 sensitization of the receptors is observed in the trace. Inset: magnification of 200
992 ms showing the initial fast desensitizing response.
993 The data from this figure containing statistical tests applied, exact sample number,
994 p values and details of replicates are available in “Figure 7 - Source Data 7”.
995

SOURCE DATA FILES FOR FIGURES:

Figure 1 - Source Data 1

Figure 2 - Source Data 2

Figure 3 - Source Data 3

Figure 4 - Source Data 4

Figure 5 - Source Data 5

Figure 6 - Source Data 6

Figure 7 - Source Data 7

Figure S1 - Source Data S1

Figure S2 - Source Data S2

SUPLEMMENTARY FILES:

Supplementary File 1

1010 **FIGURE 1**

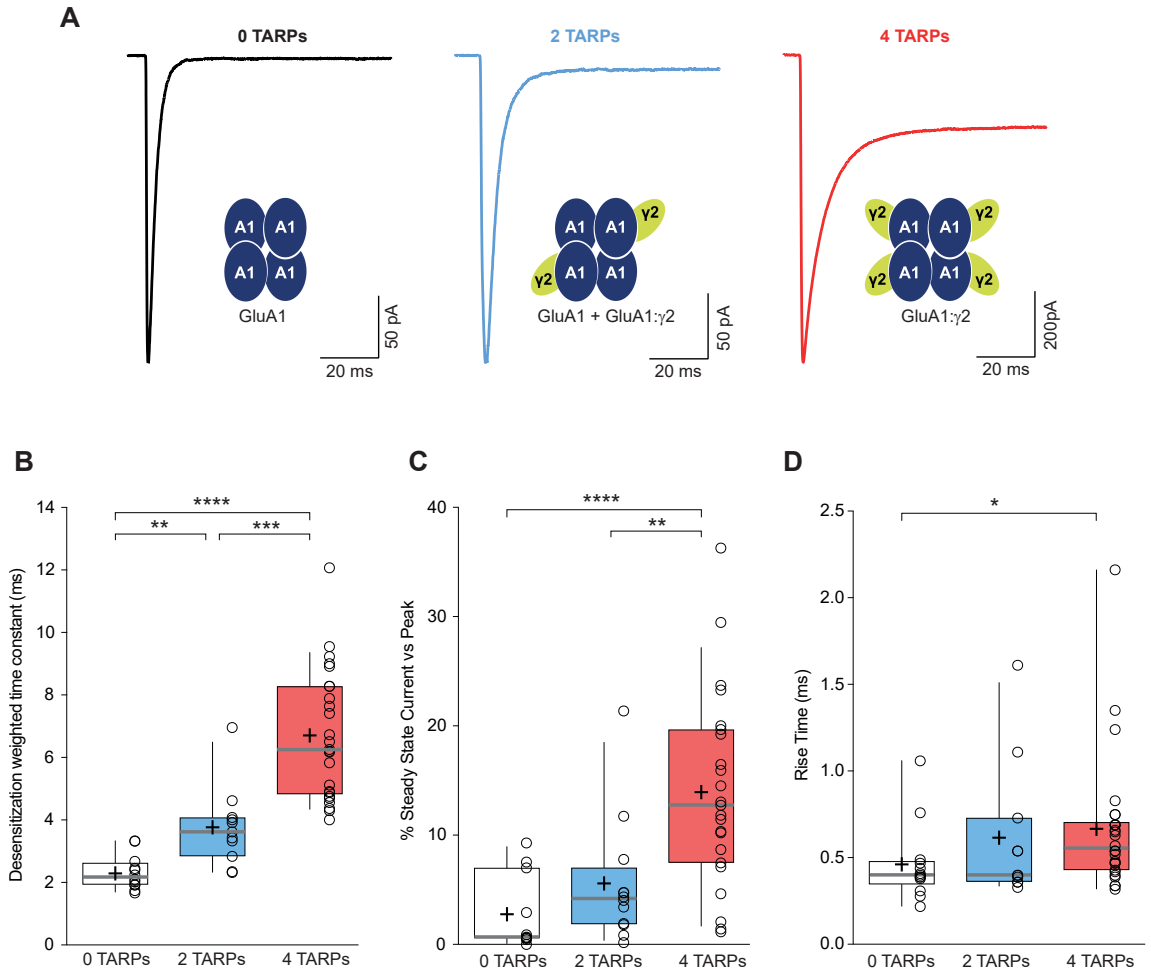

1011

1012 **Figure 1.** CP-AMPAR kinetics are differentially affected by AMPAR-TARP stoichiometry.
1013 **A.** Traces evoked at -60 mV by rapid application of 10 mM glutamate to outside-out patches
1014 from cells expressing GluA1 alone (black; average of 39 responses) or together with 2 (blue;
1015 average of 37 responses) or 4 (red; average of 67 responses) γ2 subunits. **B**. Pooled data of
1016 the weighted time constant of desensitization ($\tau_{w,\ des}$). Box-and-whisker plots indicate the
1017 median value (gray line), the 25–75th percentiles (box), and the 10–90th percentiles
1018 (whiskers); crosses and filled opened circles represent mean and the individual experimental
1019 values respectively (**p<0.01, ***p<0.001, ****p<0.0001). **C**. Pooled data showing the increase
1020 in the steady state current only in 4 TARPed CP-AMPARs (**p<0.01, ****p<0.0001). **D**. Rise
1021 time of glutamate-activated currents is only affected in a full TARPed CP-AMPAR (*p<0.05).
1022 The data from this figure containing statistical tests applied, exact sample number, p values
1023 and details of replicates are available in Supplementary File 1.

1024 **FIGURE 2**

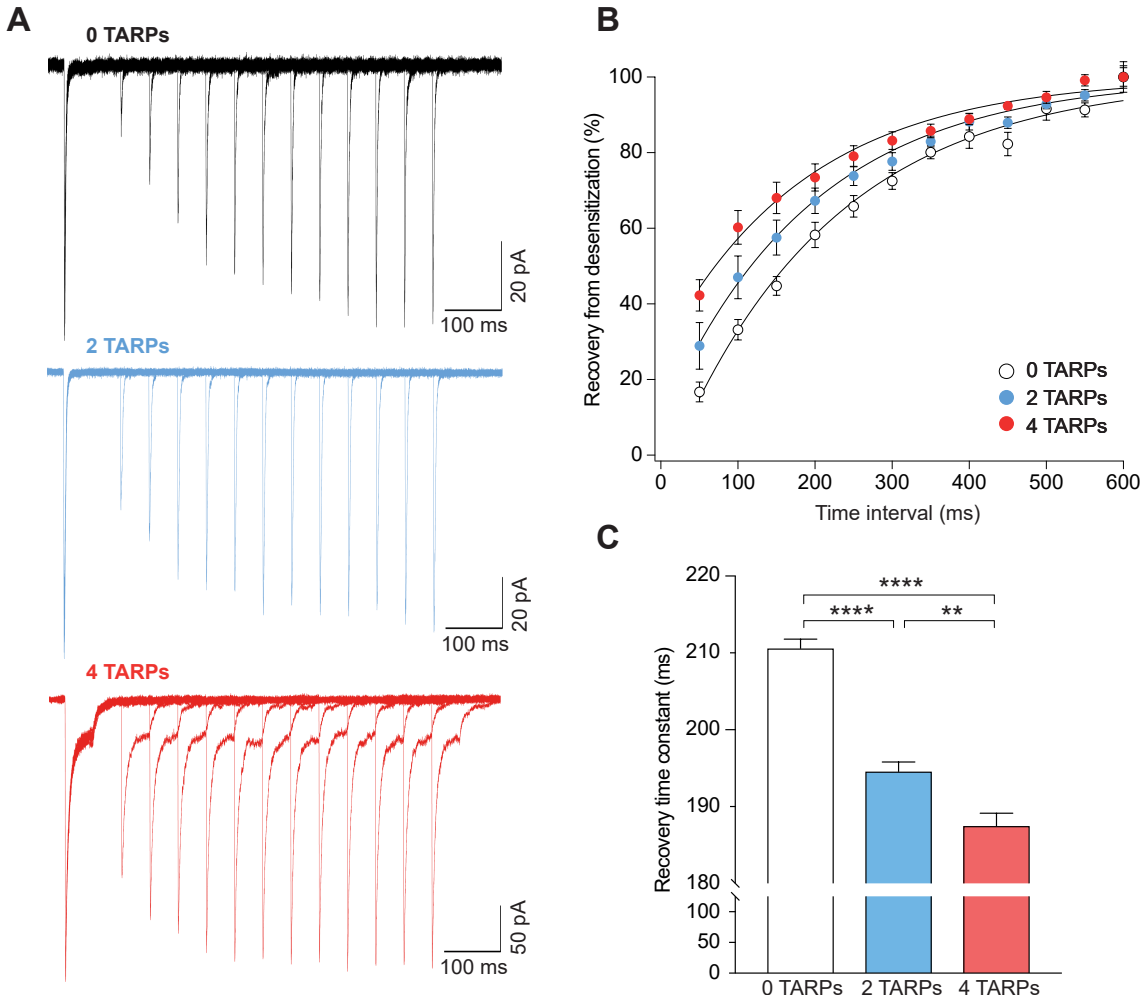

1025

1026

1027 **Figure 2.** Recovery from desensitization of CP-AMPARs is gradually enhanced with increased
1028 TARP molecules.
1029 **A**. Representative traces of a two-pulse protocol with increasing time interval between pulses
1030 for CP-AMPAR without TARPs (GluA1 homomers; black), with 2 TARPs (blue) and with 4
1031 TARPs (red). **B**. Recovery from desensitization dynamics where it can be observed the gradual
1032 diminishment in the time needed to recover as the TARP dosage increases. **C**. Recovery time
1033 constant values for the experiments showed in A and B (**p<0.01, ****p<0.0001).
1034 The data from this figure containing statistical tests applied, exact sample number, p values
1035 and details of replicates are available in Supplementary File 2.

1036

1037 **FIGURE 3**

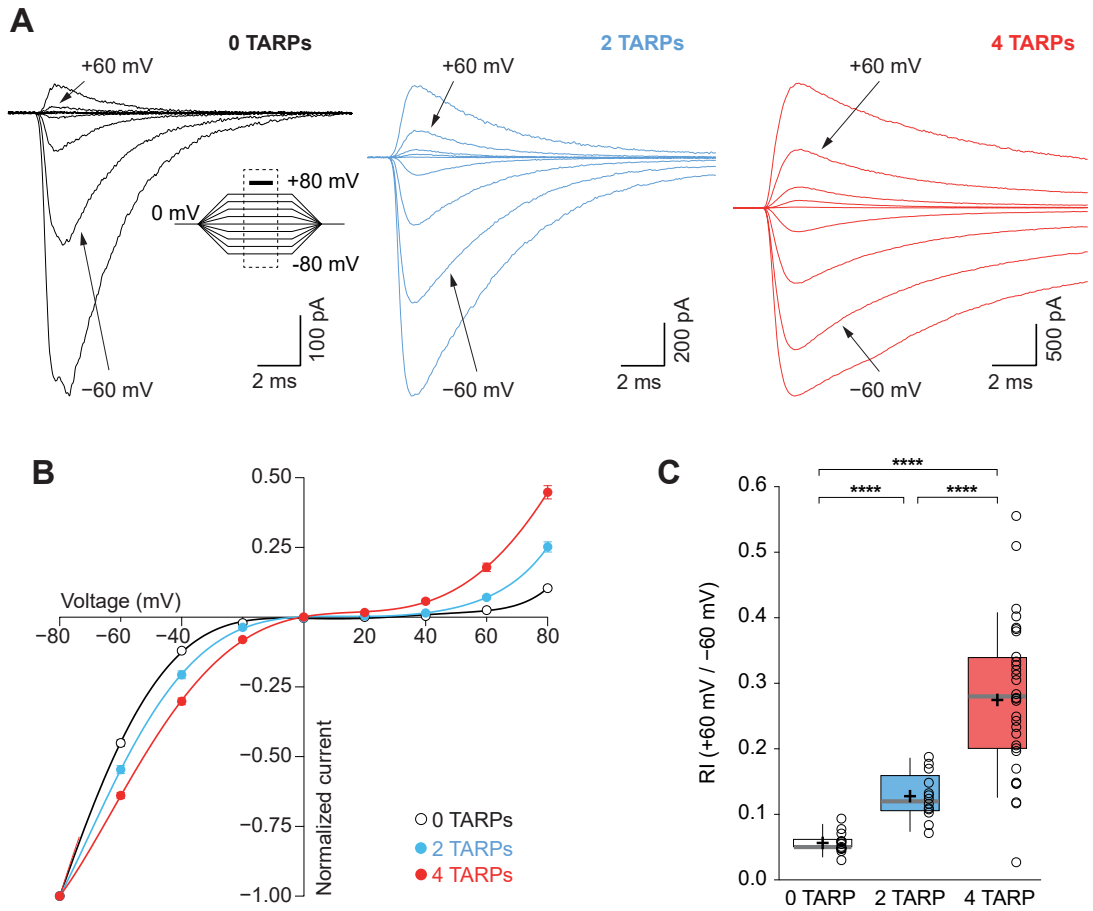

1038

1039 **Figure 3.** CP-AMPAR polyamine block attenuation is dependent on TARP dosage.

1040 **A**. Representative glutamate-evoked currents from outside-out patches at different membrane
1041 potentials from -80 to +80 in 20 mV increments from cells expressing CP-AMPARs, GluA1
1042 (black), GluA1+GluA1: γ2 (blue) and GluA1: γ2 (red). Bottom: Traces at +60 mV and -60mV
1043 membrane potentials are marked. **B**. I-V relationships constructed from glutamate-evoked peak
1044 currents of patches held at different membrane potentials in different AMPAR-TARP
1045 stoichiometries. **B**. Pooled data showing an increase in the RI as the number of TARPs per
1046 CP-AMPAR increases. The RI in 2 (blue) and 4 (red, 4 TARPed) TARPs per CP-AMPAR
1047 complex is higher compared with 0 TARPs (white, TARPless) (****p<0.0001). Box-and-
1048 whiskers plots meaning as in Figure 1.

1049 The data from this figure containing statistical tests applied, exact sample number, p values
1050 and details of replicates are available in Supplementary File 3.

1051

1052 **FIGURE 4**

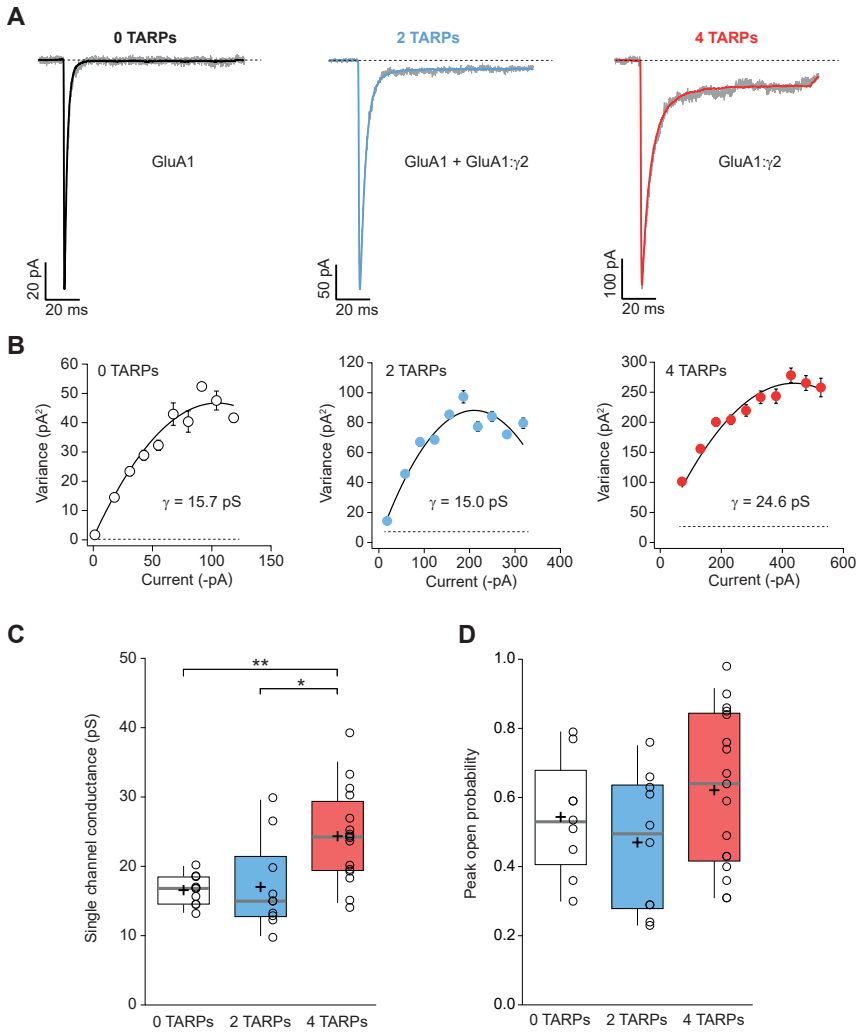

1053

1054 **Figure 4.** Four TARPs are required to increase CP-AMPAR channel conductance.
1055 **A**. Typical responses at a holding potential of -60 mV to rapid application of 10 mM glutamate
1056 to excised patches from cells expressing homomeric GluA1 alone (black; average of 84
1057 responses) or together with 2 (blue; average of 91 responses) or 4 (red; average of 223
1058 responses) γ2 subunits. A single trace is shown in gray overlaid with the mean response. **B**.
1059 Current-variance plots for the traces shown in A, the slope of which gave the weighted single-
1060 channel conductance. Broken lines show the baseline variance and error bars denote SEM.
1061 Single channel conductance values for these recordings are presented. **C**. Pooled data
1062 showing an increase of the single channel conductance only in a full-TARPed CP-AMPAR
1063 (*p<0.05, **p<0.01). **D**. Pooled data for peak open probability of CP-AMPARs. The data from
1064 this figure containing statistical tests applied, exact sample number, p values and details of
1065 replicates are available in Supplementary File 4.

1066 **FIGURE 5**

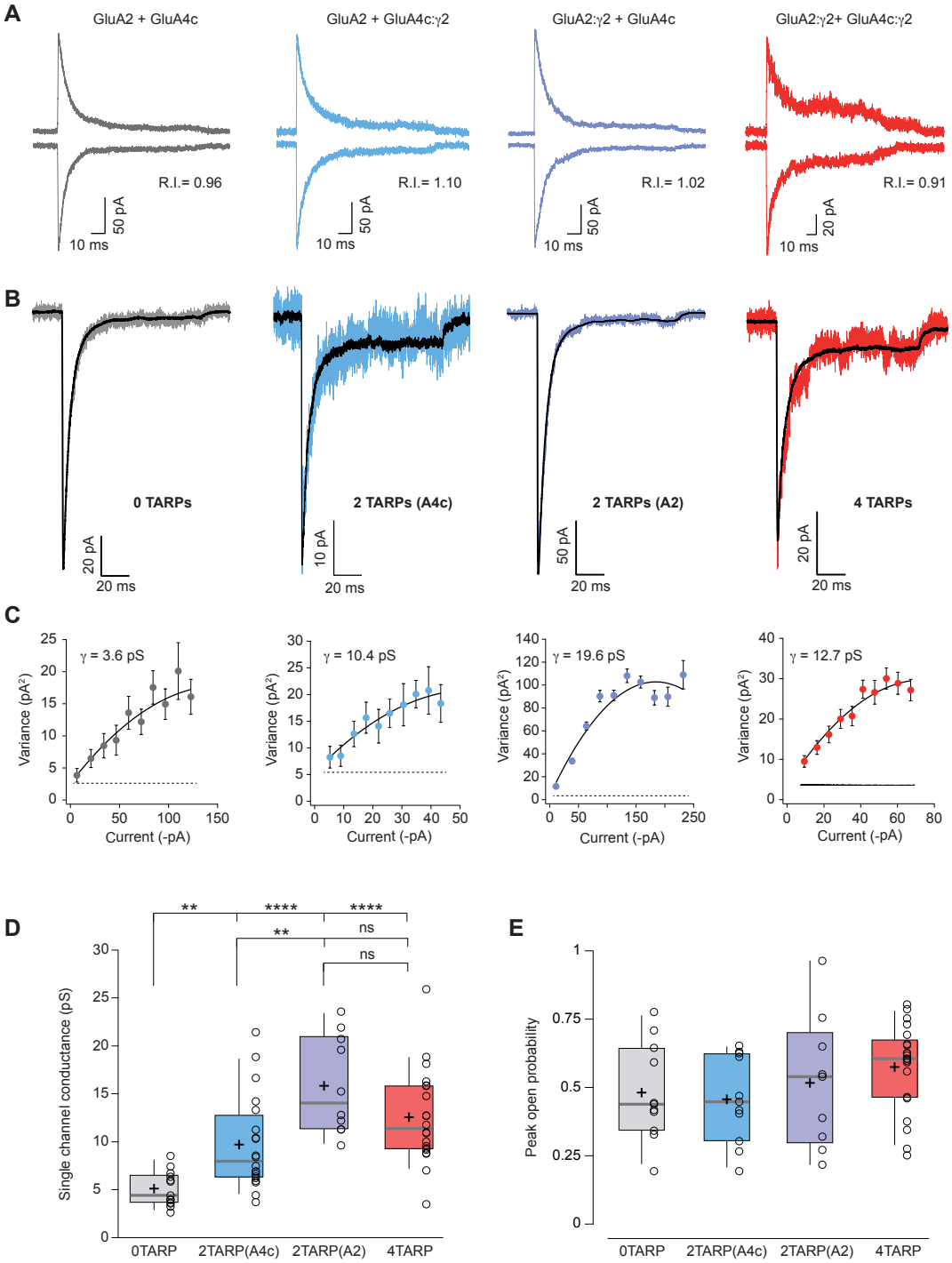

1067

1068 **Figure 5.** Single channel conductance of CI-AMPARs is modulated differently by TARPs
1069 depending on their location within the complex.
1070 **A**. Evoked currents by rapid application of 10 mM glutamate from membrane patches at +60
1071 mV (upward traces) and -60 mV (downward traces) with their corresponding RI. The

experimental conditions are designated as grey for 0 TARPs per AMPAR, blue for 2 TARPs per AMPAR with γ2 linked to GluA4c, purple for 2 TARPs per AMPAR with γ2 linked to GluA2 and red for 4 TARPs per AMPAR. **B**. Average traces of current responses evoked at -60 mV used for NSNA shown in black overlaid with a representative single response. Insets shown the studied combination. **C**. Current-variance plots for the recordings shown in B, with the weighted single-channel conductance for the single recordings. **D**. Pooled data showing a distinct degree in single channel conductance increase when γ2 is present into the AMPAR complex (*$p<0.05$, **$p<0.01$, ***$p<0.001$, ****$p<0.0001$). **E**. Pooled data for peak open probability of CI-AMPARs, where no effect of TARP stoichiometry was evident ($p>0.05$).
The data from this figure containing statistical tests applied, exact sample number, p values and details of replicates are available in Supplementary File 5.

1084 **FIGURE 6**

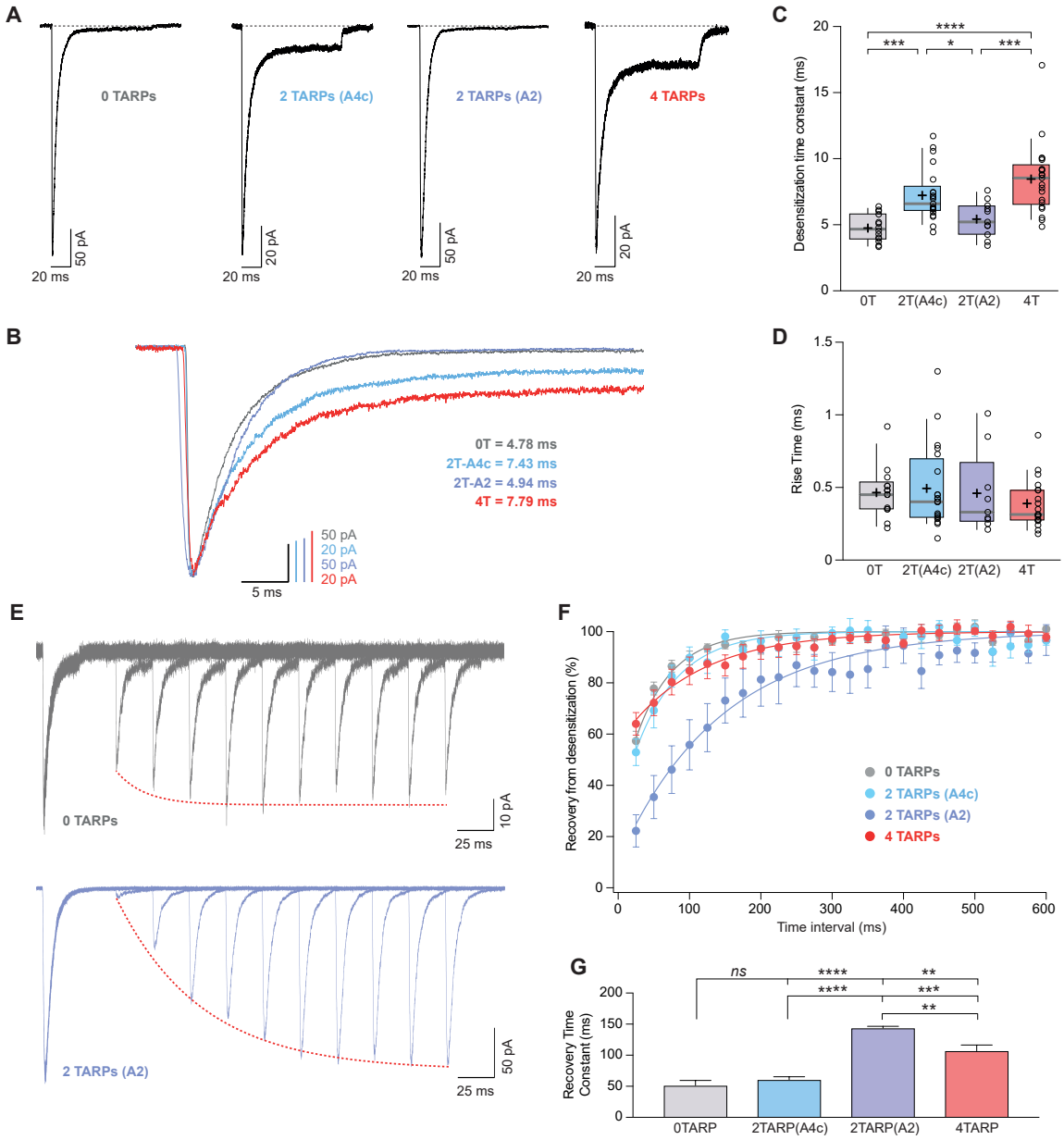

1085

1086 **Figure 6.** CI-AMPAR kinetics differ upon γ2 attachment to GluA4c or GluA2 subunit.

1087 **A**. Representative traces of currents at -60 mV from cells expressing CI-AMPARs without or
1088 with TARP γ2 linked to GluA subunits. Under the traces a scheme of the subunits forming the
1089 receptors with γ2 associated to different AMPAR subunits is shown. **B**. Peak-scaled
1090 normalization from traces shown in A for a better comparison of desensitization kinetics. **C**.
1091 Weighted time constant of desensitization ($\tau_{w,des}$) were is clear that desensitization is slowed
1092 only when γ2 is linked to GluA4c subunit (*p<0.05, ***p<0.001, ****p<0.0001).. **D**. Rise time of
1093 the current activation is not changed by the AMPAR-TARP stoichiometry. **E.** Representative

1094 traces monitoring recovery from desensitization for CI-AMPAR in cells expressing 0 TARPs or
1095 2 TARPs linked to GluA2 subunit where it is manifest the difference between the two
1096 conditions. Dashed red line: exponential fitting for the desensitization recovery. **F**. Recovery of
1097 desensitization kinetics showing a relatively slow recovery only in 2-TARPed (located in GluA2)
1098 CI-AMPARs. **G**. Recovery time constant values for the experiments showed in E and F
1099 (**$p<0.01$, ***$p<0.001$, ****$p<0.0001$).
1100 The data from this figure containing statistical tests applied, exact sample number, p values
1101 and details of replicates are available in Supplementary File 6.
1102

1103 **FIGURE 7**

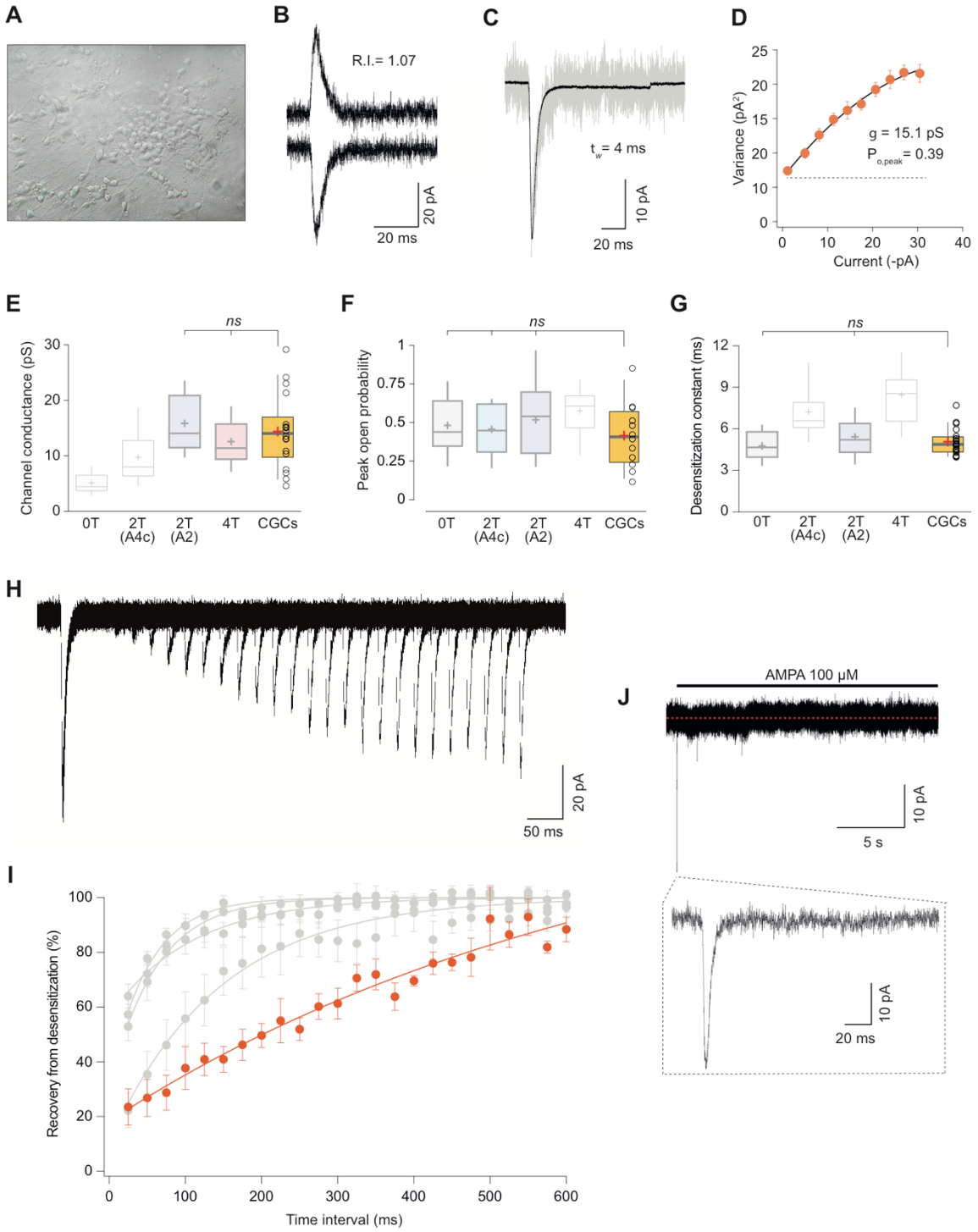

1104

1105 **Figure 7.** Somatic currents from CGCs exhibit properties of GluA2:γ2 + GluA4c CI-AMPARs.
1106 **A**. CGCs in culture after 7 days in vitro. **B**. Traces at +60mV and -60mV evoked with 100 µM
1107 AMPA from a CGC somatic patch showing the typical lineal response of a CI-AMPAR. **C**.
1108 Representative response of current evoked at -60 mV by rapid application of 100 µM AMPA to

1109 somatic patches from CGCs. Grey: representative single response; black: average of 275
1110 stable responses. **D**. NSFA from the recording in C. **E**. Data showing comparison of single
1111 channel conductance values obtained in CGCs (orange box) with recordings from transfected
1112 cell lines. The conductance values obtained resembled (without significant difference) to the
1113 ones seen with 2T (A2) or 4T conditions (marked in bold grey). **F**. Comparison of peak open
1114 probability values from CGCs were only significantly different from recordings in cell lines with
1115 4 TARPs. **G**. Compared data of desensitization time constant (ms) from CGCs with recordings
1116 in tsA201 cells. The results are no significantly different from conditions with 0T or 2T(A2). **H**.
1117 Representative trace from two-pulse protocol monitoring recovery from desensitization for
1118 CGCs somatic patches to 100 μM AMPA application. **I**. Recovery from desensitization kinetics
1119 of CGS somatic AMPARs. **J**. Representative response to a 100 μM AMPA application for 20
1120 seconds in a somatic patch from CGCs to test for the presence of γ7. No re-sensitization of the
1121 receptors is observed in the trace. Inset: magnification of 200 ms showing the initial fast
1122 desensitizing response.
1123 The data from this figure containing statistical tests applied, exact sample number, p values
1124 and details of replicates are available in Supplementary File 7.
1125

1126 **FIGURE S1**

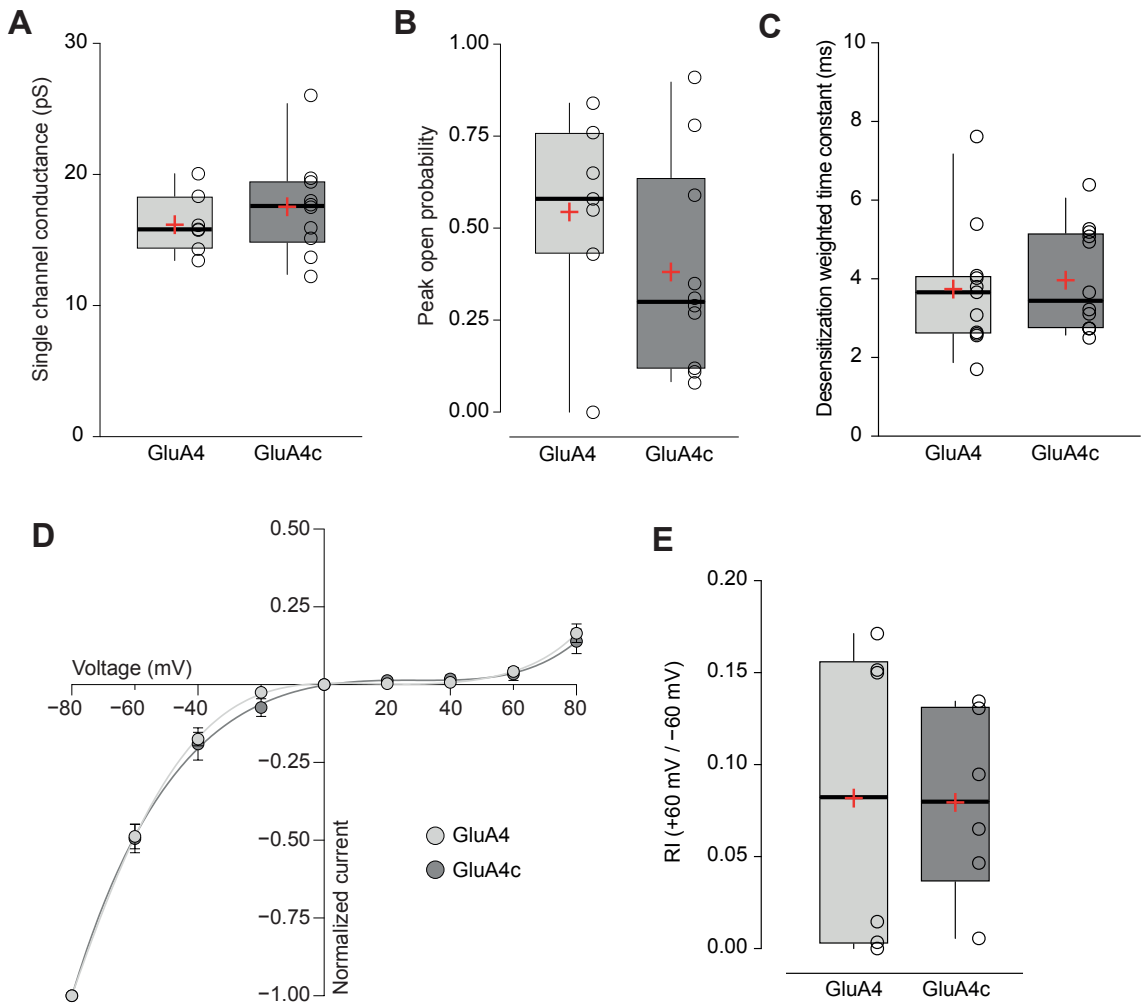

1127

1128 **Figure S1**: Short and long isoforms of GluA4 show the same electrophysiological behaviour.
1129 **A**. Pooled data showing single channel conductance from GluA4 (light grey) and GluA4c (dark
1130 grey) homotetramers. Box-and-whiskers plots represent percentiles, median and average as
1131 stated in Figure 1c. **B**. Data showing peak open probability from GluA4 and GluA4c tetramers
1132 using the same colour pattern as in figure 5a. **C**. Weighted time constant of desensitization ($\tau_{w,des}$)
1133 from GluA4 and GluA4c tetramers. **D**. Inwardly rectifying I-V relationships constructed
1134 from peak currents evoked by glutamate (100 ms, 10 mM) applied to outside-out patches from
1135 tsA201 cells containing GluA4 (light circle) or GluA4c (dark circle). Fittings are adjusted to a 6th
1136 order polynomial function. **E**. RI (+60mV/-60mV) values from GluA4 and GluA4c tetramers.
1137 The data from this figure containing statistical tests applied, exact sample number, p values and
1138 details of replicates are available in "Figure S1 - Source Data S1".
1139

1140 **FIGURE S2**

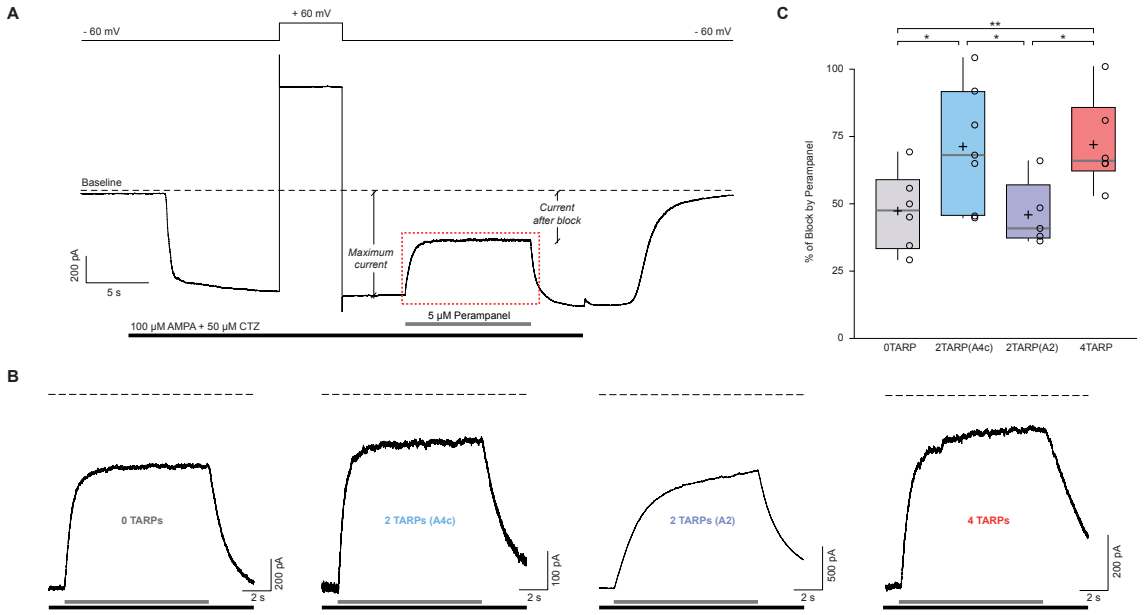

1141

1142 **Figure S2**: The block of the non-competitive antagonist perampanel varies with AMPAR-TARP
1143 stoichiometry. **A**. Representative whole-cell recording showing the protocol used to determine
1144 the percentage of perampanel block. This trace corresponds to a cell expressing GluA2 and
1145 GluA4c. Cells were clamped at -60 mV during the recording with a 5 second pulse duration at
1146 +60 mV to asses for GluA2 presence. Black bar shows application time of AMPA 100 µM +
1147 Cyclothiazide 50 µM to tsA201 cells expressing different AMPAR-TARP combinations. Grey
1148 bar shows rapid application (< 1ms) of Perampanel at 5µM. Baseline is pointed with dashed
1149 line. Maximum current and current after block are displayed. The dashed red frame represents
1150 the magnification part shown in panel b. **B**. Representatives traces of Perampanel blocking
1151 from each condition following the same colour pattern as in Figure 5. Under each trace the
1152 black bar shows AMPA + CTZ and grey bar shows application of Perampanel. **C**. Pooled data
1153 for the percentage of blocking by Perampanel. Box-and-whiskers plots as in Figure 1c. The
1154 data from this figure containing statistical tests applied, exact sample number, p values and
1155 details of replicates are available in “Figure S2 - Source Data S2”.

1156

1157 **Supplementary Material and Methods**

1158

1159 1.1 Animals and housing

1160 C57BL/6N wild-type mice were housed in cages with free access to food and water
1161 and were maintained under controlled day–night cycles in accordance with the NIH
1162 Guide for the Care and Use of Laboratory Animals, the European Union Directive
1163 (2010/63/EU), and the Spanish regulations on the protection of animals used for
1164 research, following a protocol approved and supervised by the CEEA-UB (Ethical
1165 Committee for Animal Research) from University of Barcelona with the license
1166 number OB117/16, of which DS is the responsible researcher.

1167

1168 1.2 Cell lines culture and transfection

1169 In this study, we have used tsA201 cells, a cell line derived from HEK293 cells
1170 stably transfected with the temperature sensitive gene for SV40 T-antigen to allow
1171 plasmid replication using the SV40 origin and hence to produce high levels of
1172 recombinant proteins (Sigma catalog #85120602). Cells were maintained as
1173 described in Gratacòs-Batlle et al., 2015 [29].

1174

1175 Cells were plated into poly-D-lysine coated coverslips 24 h before transfection at a
1176 density of 1.5×10^6 cells/coverslips. Cells were then transiently transfected with
1177 0.8-1 µg total cDNA using PEI reagent (1 mg/ml) in a 3:1 ratio (PEI:DNA) according
1178 to the manufacturer's directions. The ratio of cDNA used in each condition varied
1179 depending on the set of experiments.

1180

1181 1.3 Constructs

1182 GluA1, GluA2 and GluA4 cDNAs (rat, flip isoforms) were old gifts from S.
1183 Heinemann (Salk Institute, La Jolla, CA, USA) and P. Seeburg (Max Planck
1184 Institute, Heidelberg, Germany).

1185

1186 For this work we used the short version of GluA4, namely GluA4c – first described
1187 in 1992 [30] – in its flip form. The GluA4c subunit was cloned from mRNA obtained

1188 from adult rat cerebellum (*Rattus norvegicus*) cerebellum into a pIRES-mCherry
1189 plasmidic vector. The primers used were the following:
1190
1191 Primer Forward (5'-3'): GCGC GCT AGC ATG AGG ATT TGC AGG CAG ATT
1192 (GCGC GCT AGC restriction site cloned using NheI-HF enzyme, catalog: NEB
1193 #R3131S).
1194
1195 Primer Reverse (5'-3'): CGCGG CTC GAG ATT CTT AAT ACT TTC GGT TCC A
1196 (CGCGG CTC GAG restriction site cloned using XhoI-HF enzyme, catalog: NEB
1197 #R0146S).
1198
1199 GluA1:γ2 and GluA2:γ2 tandem proteins (into pIRES-GFP vectors) were a
1200 generous gift from Ian Coombs (UCL, London, UK). GluA4c:γ2 tandem was
1201 subcloned into a pIRES-mCherry vector from the GluA4c and the γ2 plasmidic
1202 vectors. All constructs have been fully sequenced.
1203
1204 1.4 Electrophysiology
1205
1206 1.4.1 Whole-cell recordings
1207 Whole-cell recordings were made from isolated cells using electrodes with a
1208 resistance of 3–5MΩ, giving a final series resistance of 5–15 MΩ. Voltage was held
1209 at -60 mV unless otherwise stated. Currents were low-pass filtered at 2 kHz and
1210 digitized at 5 kHz. Receptors were activated by bath application of 10 mM
1211 glutamate plus 50 μM cyclothiazide (CTZ) to prevent receptor desensitization.
1212
1213 1.4.2 Fast agonist application into outside-out patches
1214 Outside-out patches were obtained using electrodes with a resistance of 5–10 MΩ.
1215 Rapid solution switching at the patch was carried out by piezoelectric translation of
1216 a theta-barrel application tool made from borosilicate glass (1.5mm o.d.; Sutter
1217 Instruments) mounted on a piezoelectric translator (P-601.30; Physik Instrumente).
1218 Control and agonist solutions flowed continuously through the two barrels of the

theta glass and solution exchange occurred when movement of the translator was triggered by a voltage step (pClamp). To enable visualization of the solution interface and to allow measurement of the solution exchange 2.5 mg/ml sucrose was added to the agonist solution and the control solution was diluted by 4%. Currents were activated by 10mM glutamate and were low-pass filtered at 10 kHz and digitized at 50 kHz. At the end of each experiment, the adequacy of the solution exchange was assessed by destroying the patch and measuring liquid-junction current at the open pipette; the 10–90% rise time was always <400 µs.

1.4.3 Recovery from desensitization

To study AMPAR recovery from desensitization, a two-pulse protocol (25 ms each) was used in which a first pulse was applied followed by a second pulse at different time intervals (from 25 ms to 625 ms). The paired pulses were separated 1s to allow full recovery from desensitization. To estimate the percentage of recovery, the magnitude of peak current at the second pulse (P2) was compared with the first one (P1).

1.4.4 Non-stationary fluctuation analysis (NSFA)

To infer channel properties from macroscopic responses, glutamate (10 mM) was applied onto outside-out patches (100 ms duration at 1 Hz) and the ensemble variance of all successive pairs of current responses was calculated using IGOR Pro 6.06 (Wavemetrics, OR) and NeuroMatic [33]. The single-channel current (*i*), total number of channels (N) and maximum open probability ($P_{o,max}$) were then determined by plotting this ensemble variance (σ^2) against mean current (I) and fitting with a parabolic function:

$$\sigma^2 = \sigma_B^2 + \left(iI - \left(\frac{I^2}{N} \right) \right)$$

where σ_B^2 is the background variance. Along with the expected peak-to-peak variation in the currents due to stochastic channel gating, some responses showed

a gradual decrease in peak amplitude (*run-down* of the current). The mean response was calculated from epochs containing 50 to 350 stable responses, which were identified by using a Spearman rank-order correlation test (NeuroMatic). The weighted-mean single-channel conductance was calculated from the single-channel current and the holding potential (being -0.055 V after corrected for liquid-junction potential). $P_{o,max}$ was estimated by dividing the average peak current by theoretical maximum current (*i*N).

1.4.5 Kinetics of desensitization

The kinetics of desensitization of glutamate-evoked responses and the kinetics of recovery from desensitization were fitted according to a double-exponential function to calculate the weighted time constant ($\tau_{w,des}$):

$$\tau_{w,des} = \tau_f \left(\frac{A_f}{A_f + A_s}\right) + \tau_s \left(\frac{A_s}{A_f + A_s}\right)$$

where A_f and τ_f are the amplitude and time constant of the fast component of recovery and A_s and τ_s are the amplitude and time constant of the slow component.

1.4.6 Current-voltage relationships

In order to study the degree of spermine block of CP-AMPARs at different membrane potentials we applied 10 mM glutamate onto outside-out membrane patches at different holding potentials (from −80 mV to +80 mV in 20 mV increments) and the peak current was used to construct the current-voltage relationship.

The rectification index (*RI*) was defined as the absolute value of glutamate-evoked current at +60 mV divided by that at −60 mV:

$$RI_{+60mV/-60mV} = \frac{|I_{+60mV}|}{|I_{-60mV}|}$$